Arabian Journal for Science and Engineering (2019) 44:8265–8288
https://doi.org/10.1007/s13369-019-03867-x

RESEARCH ARTICLE - CIVIL ENGINEERING

Probabilistic Behavior Assessment of Base-Isolated Buildings and Base Isolation Systems Subjected to Various Earthquakes with Different Components

Mohammad Reza Bagerzadeh Karimi[1] · **Mehmet Cemal Geneş**[1]

Received: 7 November 2018 / Accepted: 17 April 2019 / Published online: 17 June 2019

Abstract
One of the greatest challenges of researchers is to understand the behavior of base isolation systems and base-isolated buildings under the conditions of different ground motions. The specific objective of this study is to evaluate the seismic response of multi-story base-isolated buildings with lead core rubber bearings (LCRBs) and buildings that are not isolated when subjected to different types of ground motions with different components. Under these conditions, the equations of motion of buildings with isolation systems are obtained, and LCRB force–deformation behavior is modeled as bilinear in MATLAB. Then, the behaviors of the base isolation system and base-isolated buildings are evaluated for 45 different earthquake scenarios, which are categorized into three different groups with regard to the ratio of peak ground acceleration to peak ground velocity (PGA/PGV). The dissipation of energy by a base isolation system, which is induced by the earthquake, varies for three different ranges of the PGA/PGV ratio. Despite the fact that by increasing the number of stories, the effectiveness of the isolator system decreases, this paper shows the most important finding to be that the damage limitation requirement is kept below 1% according to Eurocode 8, which is the requirement for buildings at the upper limit on the inter-story drift ratio under seismic loading, and the inter-story drifts significantly decreases for the *base-isolated* buildings and even for high-rise buildings.

Keywords Damage limitation · Two-factor factorial design · Lead core rubber bearing · Probabilistic evaluation · Seismically isolated building

List of Symbols

M	Mass matrix
m_b	Mass of the base slab
m_t	Total mass
C	Damping matrix
c_b	Damping of the isolator
K	Stiffness matrix
k_b	Isolator force divided by the maximum displacement
k_p and k_i	Post- and pre-yielding stiffnesses of the bearing, respectively
r	Unit vector
u	Displacement vector
$\ddot{u}_\mathrm{g}$ or $\ddot{x}_\mathrm{g}$	Longitudinal earthquake acceleration
$\ddot{u}_\mathrm{b}$	Relative acceleration of the base slab
a_0 and b_0	Proportional coefficients
ω_i and ω_j	Structural modal frequencies
ξ_i and ξ_j	Structural damping ratio
ξ_b	Isolator damping ratio
F_b	Restoring force
α_1	Post- to pre-yielding stiffness ratio
T_b	Isolation period
T_s	Period of the superstructure
ω_b	Isolator frequency
z	Nondimensional hysteretic displacement component
f_y	Yield strength of the bearing
u_y	Yield displacement

✉ Mohammad Reza Bagerzadeh Karimi
mohammad.karimi@cc.emu.edu.tr

Mehmet Cemal Geneş
cemal.genes@emu.edu.tr

[1] Civil Engineering Department, Eastern Mediterranean University (EMU), Famagusta, North Cyprus Via Mersin 10, Turkey

D	Maximum displacement
Q	Characteristic strength where the isolator hysteresis loop intercepts the axis
f_0	Normalized yield strength
W	Total building weight
h	Story height
g	Gravitational acceleration
N	Number of stories
γ_1	Importance factor
a_{gR}	Reference peak ground acceleration

Abbreviations

FBB	Fixed-base building
BIB	Base-isolated building
PGA	Peak ground acceleration
PGV	Peak ground velocity
PGD	Peak ground displacement

1 Introduction

In a base-isolated building, the building is physically separated from the ground. When an earthquake occurs, the period shifts and causes a reduction in the acceleration of the floor and inter-story drift on the superstructure, which can be compared with a building that is not isolated. As the responses are reduced, it allows the building to remain in the elastic or close to elastic region according to the design level event. Simultaneously, reductions in acceleration and drift demands, which are gained by seismic isolation systems, make it one of the most useful tactics to achieve better performance following strong and infrequent earthquake events. Since the development of the base isolation method, several isolation devices have been suggested, implemented and studied, especially focusing on their capacity to carry vertical loads and withstand large horizontal deformations.

Several interesting studies have been conducted on base-isolated structures and base isolation systems under different seismic activities [1–7]. However, the fact is that the base isolation systems and base-isolated buildings are highly affected by ground motion characteristics and may behave differently for different seismic events. Alhan et al. [8] noted the performance limit of base-isolated buildings subjected to various near-field ground motions with different velocity pulse periods. Although the isolation system may be effective under far-field ground motions, it is still complicated for near-field ground motions. It was also illustrated that the proportion of the base isolation period to the pulse period of ground motions (T_b/T_p) considerably affects the displacement of the base and the acceleration of the story for long and short pulse periods, respectively. In addition, this was found for small ratios of the base isolation system period to pulse period and for shorter fault distances. Matsagar et al. [9] illustrated that the responses of multi-story base-isolated buildings are affected by different characteristic parameters of isolator. The shape of the force–deformation behavior of the isolator, which affects the responses of the base-isolated structure, is investigated under the main varied parameters, such as the yield displacement of the isolator, flexibility of the superstructure, time period of the isolator and number of stories of the base-isolated structure. It was found that the form of the hysteresis loop of the isolation system considerably affects the responses of the base-isolated buildings. In addition, Samali et al. [10] carried out a case study with an experimental setup on a shake table. In their research, a mass modeled with eccentricity above the base isolation system was considered. Therein, the dynamic behavior of a five-story benchmark building with mass eccentricity under four different earthquake scenarios was investigated. Moreover, it was demonstrated that the related base isolation system behaves ineffectively under some kinds of earthquakes.

Jangid [11] assessed the behavior of the LCRB system for multi-story buildings subject to near-fault ground motions. In his study, the response of the system under six different ground motions was evaluated, and variations in top floor absolute accelerations and bearing displacements of the multi-story base-isolated building were examined and illustrated. As a result, the yield strength (f_y) of the LCRB was found to be between 10 and 15% of the building weight under different ground motions. Mavronicola [12] studied two special cases of isolated building responses during seismic activities. First, the nonlinear behavior of the lead rubber bearing and, second, a base-isolated building with an adjacent structure were investigated when subjected to very strong earthquakes. The relative displacements of the isolator were underestimated, and the peak floor accelerations were overestimated by the bilinear model. Chimamphant et al. [13] proposed 3-, 9- and 20-story base-isolated and fixed-base buildings (MDOF shear beam models), and the effects of such essential structural parameters, such as the isolator stiffness, the damping ratio of the isolator and the number of stories, on the responses of the base-isolated buildings were studied parametrically. It was discovered that the return period may be very sensitive to short buildings and less sensitive to tall buildings. Takewaki et al. [14] investigated the strength of the base-isolated tall buildings with the code defined for ground motions. They considered two kinds of base isolation systems, namely linear or natural rubber bearings and friction-type bearings. In their assessment, the inverse problem was generated for the targeted drift of the base-isolated building to specify the required amount of additional viscous damping. As the height of the base-isolated building increases, the damping ratio decreases. Moreover, it was concluded that

high-rise buildings that are base-isolated have low resistance against ground motions than base-isolated low-rise buildings.

While some research has been carried out on different types of isolation systems, there is still very little scientific understanding of the behavior of the LCRB control systems when induced by different ground motions for a varied number of buildings. However, previous studies have stated that the effectiveness of the isolator system decreases by increasing the number of stories, but this paper demonstrates the most important discovery that the damage limitation requirement is kept below 1% according to Eurocode 8 under varied seismic loading and that inter-story drifts are significantly decreased even for base-isolated high-rise buildings.

For this reason, to better determine the performance of the base isolation system and base-isolated buildings, a set of 45 earthquakes was selected from the Pacific Earthquake Engineering Research (PEER) center database with different PGA-to-PGV ratios. In this investigation, different types of buildings (isolated and nonisolated), with 5, 10, 15, 20, 25, 30 and 35 stories, were considered and assumed that the superstructure remained linear–elastic throughout the time-history analyses. Bearing in mind that both the acceleration and velocity characteristics of an earthquake are very important parameters affecting a building (both in the base-isolated and nonisolated states), these two parameters with their ratios are considered in this study. The ratios are categorized as PGA/PGV < 1, $1 <$ PGA/PGV < 2 and PGA/PGV > 2. To conduct the numerical analysis, a MATLAB-based code is used to assess the aforementioned parameters. Additionally, a two-factor factorial design is implemented to interpret the results using Minitab software. The results clearly depict the behavior of the LCRB system under the aforementioned earthquakes when used for varied buildings. Finally, the performances of the base isolation system and base-isolated buildings are compared.

2 Governing Equations of Motion

According to Fig. 1, to investigate the behavior of the isolators and base-isolated buildings, the mathematical model of a multi-story (with N number of stories) isolated building with LCRBs is idealized as a two-dimensional frame. For this frame, the equations of motion for a fixed-base building can be shown as [15]:

$$\mathbf{M}\ddot{u} + \mathbf{C}\dot{u} + \mathbf{K}u = -\mathbf{M}r\ddot{u}_{\mathrm{g}} \tag{1}$$

In Eq. (1), $\mathbf{M}$, $\mathbf{C}$ and $\mathbf{K}$ are the mass, damping and stiffness matrices ($n \times n$ matrices) of the superstructure, respectively; u is the $n \times 1$ vector, which is the relative displacement of the building with respect to the ground, and the dot above u refers to the time derivative; r is the unit vector, which is the $n \times 1$ matrix in the direction of the ground motion; and $\ddot{u}_{\mathrm{g}}$ is the acceleration of the ground motion. The structural damping matrix C is assumed to be the mass proportional damping and stiffness proportional damping (Rayleigh damping), as given in the following:

$$\mathbf{C} = a_0\mathbf{M} + b_0\mathbf{K} \tag{2}$$

where $a_0 = \xi_i \frac{2\omega_i\omega_j}{\omega_i+\omega_j}$ and $b_0 = \xi_j \frac{2}{\omega_i+\omega_j}$ are damping proportional coefficients; ω_i and ω_j are structural modal frequencies; and ξ_i and ξ_j are structural damping ratios for modes i and j, respectively.

For a seismically isolated building with a base mass (m_{b}), the governing equations of motion of the isolated building can be written as [15]:

$$\mathbf{M}\ddot{u} + \mathbf{C}\dot{u} + \mathbf{K}u = -\mathbf{M}r\left(\ddot{u}_{\mathrm{g}} + \ddot{u}_{\mathrm{b}}\right) \tag{3}$$

As aforementioned, u is the displacement vector with respect to the base raft in the building and $\ddot{u}_{\mathrm{b}}$ is the isolator acceleration with respect to the ground. Thus, the base slab equation of motion can be shown as follows [15]:

$$m_{\mathrm{b}}\ddot{u}_{\mathrm{b}} + c_{\mathrm{b}}\dot{u}_{\mathrm{b}} + F_{\mathrm{b}} - k_1u_1 - c_1\dot{u}_1 = -m_{\mathrm{b}}\ddot{u}_{\mathrm{g}} \tag{4}$$

where F_{b} (restoring force) is developed in the isolator system (Fig. 1c); c_{b} is damping of the isolator; k_1 and c_1 are the stiffness and damping of the first floor, respectively; u_1 and $\dot{u}_1$ are the displacement and velocity of the first floor, respectively; and m_{b} is the mass of the base slab.

2.1 Lead Core Rubber Bearing (LCRB)

In 1975, LCRBs were found in New Zealand and were also widely used in Japan and the USA. These systems are generally known as N–Z or LCRB systems. These bearings (NZ or LCRB) are similar to natural rubber bearing systems that have no central lead core, but to dissipate extra energy and increase the primary resistance against minor ground motions and winds, a central lead core is used inside them [15]. This system essentially behaves as a hysteretic damping device. Bilinear force–deformation hysteresis of the LCRB is illustrated in Fig. 1c. For the present study, the Bouc Wen model [16] is used to determine the hysteretic behavior of the LCRB, as shown schematically in Fig. 1b, c. In addition, with regard to the governing equation (Eq. (4)), implementation of the restoring force for the isolation bearing is considered as [16]:

$$F_{\mathrm{b}} = \alpha_1 k_i u_{\mathrm{b}} + (1-\alpha_1)k_i u_{\mathrm{y}} z \tag{5}$$

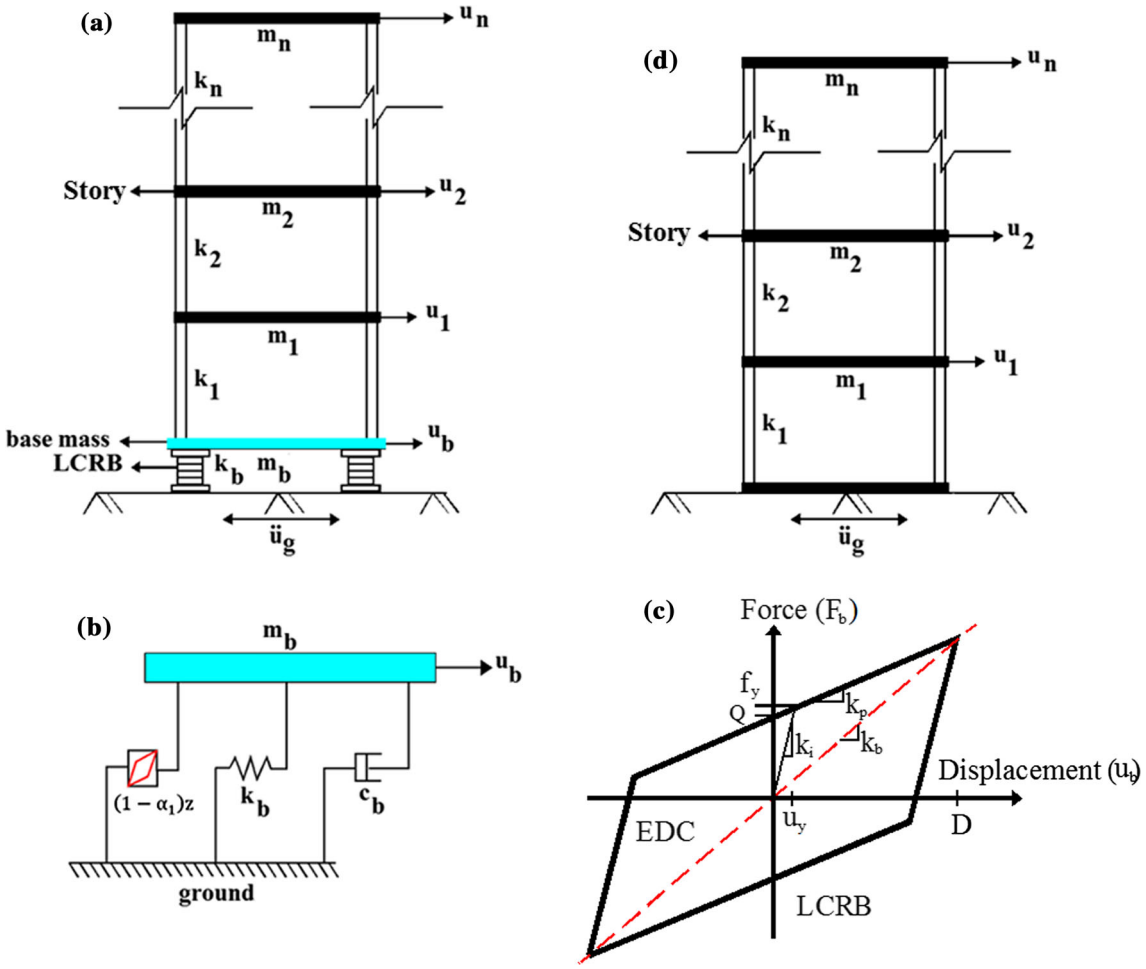

Fig. 1 Idealized model of a multi-story structure: **a** base-isolated building (BIB); **b** idealization of the LCRB isolator; **c** bilinear force–deformation hysteresis of LCRB; and **d** fixed-base building (FBB)

where $f_y = k_i u_y$ is the yielding force of the isolator, and it is a point where the initial stiffness (pre-yielding stiffness) changes to secondary stiffness (post-yielding stiffness); u_y is the yielding displacement. k_i is the pre-yielding stiffness of the LCRB, usually at a displacement of less than 25.4 mm. The value of this parameter is affected by the lead core size, which is important for controlling the responses under the service loads. k_b is the stiffness of the LCRB, which is related to the modulus, area of the rubber and total height of the isolator and can also be calculated using Eq. (6). k_P and k_i are the post- and pre-yielding stiffnesses of the bearing, respectively; α is the ratio of the post-yielding stiffness to pre-yielding stiffness ($\alpha_1 = \frac{k_P}{k_i}$); and u_b is the isolator displacement with respect to the ground.

The LCRB system is defined by ξ_b, T_b and f_0 parameters, which are the damping ratio of the isolation system, the period of the isolator and the normalized yield strength (i.e., $f_0 = \frac{Q}{W}$), respectively (where $W = m_t g$, W is the weight of the building together with a base raft (m_b) and g is the acceleration due to gravity) [11, 12, 17]. Q is the characteristic strength where the isolator hysteresis loop intercepts the axis (Fig. 1c).

$$k_b = \frac{m_t}{\left(\frac{T_b}{2\pi}\right)^2} \tag{6}$$

$$c_b = 2 m_t \omega_b \xi_b \tag{7}$$

where m_t is the mass of the superstructure together with a base raft (m_b) which is specified in Eq. (8), and $\omega_b = \frac{2\pi}{T_b}$ is the isolator frequency. For the bilinear response shown in Fig. 1c, ξ_b can be calculated using $\xi_b = \frac{2Q(D-u_y)}{\pi k_b D^2}$, where the parameters are identified in Fig. 1c [18].

$$m_t = m_b + \sum_{i=1}^{N} m_i \tag{8}$$

In Eq. (9), z is a hysteretic displacement component that is nondimensional and satisfies the following differential equation expressed as a nonlinear first-order equation [16]:

$$\dot{z} = u_{\mathrm{y}}^{-1}\left(A\dot{u}_{\mathrm{b}} - \beta|\dot{u}_{\mathrm{b}}||z|^{n-1}z - \gamma\dot{u}_{\mathrm{b}}|z|^{n}\right) \tag{9}$$

The parameters of γ,β, A are dimensionless, and n should be selected such that the responses from the model exactly match the experimental outputs. n is constant, which controls the changes from elastic to plastic response. In this study, the other parameters of the LCRB are held constant with $\beta = \gamma = 0.5, A = 1\,(\frac{A}{\gamma+\beta} = 1)$and $n = 2$ [16]. EDC (Energy Dissipated per Cycle) can be measured by calculating the area under the force–deformation loop, which denotes the damping value of the isolator (Fig. 1c).

2.2 Solution Procedures for the Equations of Motion

The solutions of Eqs. (1) and (3) are performed using the Runge–Kutta method by solver ode45 in MATLAB. ode45 is based on the Runge–Kutta (4,5) formula, which is mostly used as a first attempt to solve the problem [19]. The function is utilized for the time integration procedure at an equal time interval of Δt.

For a conventionally fixed-base structure, the equation of motion is given by Eq. (1). By placing the structural model on a base isolation system (Fig. 1a), which consists of base mass (m_{b}), stiffness (k_{b}) and damping (c_{b}), Eq. (1) changes to Eq. (3).

The equation of motion for the building combined with a base raft (with isolator) can be written as:

$$r^{T}M\left(\ddot{u} + r\ddot{u}_{\mathrm{b}} + r\ddot{u}_{\mathrm{g}}\right) + m_{\mathrm{b}}\left(\ddot{u}_{\mathrm{b}} + \ddot{u}_{\mathrm{g}}\right) + c_{\mathrm{b}}\dot{u}_{\mathrm{b}} + k_{\mathrm{b}}u_{\mathrm{b}} = 0 \tag{10}$$

which can also be shown in the following form:

$$r^{T}M\ddot{u} + (m_{t})\ddot{u}_{\mathrm{b}} + c_{\mathrm{b}}\dot{u}_{\mathrm{b}} + k_{\mathrm{b}}u_{\mathrm{b}} = -(m_{t})\ddot{u}_{\mathrm{g}} \tag{11}$$

Equation (11) identifies $r^{T}M$ as the overall mass of the superstructure; therefore, $m_{\mathrm{t}} = m + m_{\mathrm{b}}$ is the overall mass carried by the isolator. The matrix form of this equation is:

$$\mathbf{M}^{*}\ddot{u}^{*} + \mathbf{C}^{*}\dot{u}^{*} + \mathbf{K}^{*}u^{*} = -\mathbf{M}^{*}r^{*}\ddot{u}_{\mathrm{g}} \tag{12}$$

where $\mathbf{M}^{*} = \begin{bmatrix} m + m_b & r^{T}M \\ Mr & M \end{bmatrix}$, $\mathbf{C}^{*} = \begin{bmatrix} c_{\mathrm{b}} & 0 \\ 0 & C \end{bmatrix}$, $\mathbf{K}^{*} = \begin{bmatrix} k_{\mathrm{b}} & 0 \\ 0 & K \end{bmatrix}$, $r^{*} = \begin{bmatrix} 1 \\ 0 \end{bmatrix}$, $u^{*} = \begin{bmatrix} u_{\mathrm{b}} \\ u \end{bmatrix}$, $m = \sum_{i=1}^{N} m_i$

2.3 Program Validation

The validity of the program was confirmed by comparing the results obtained from the following studies:

Chao Xu et al. [17] studied a three-story base-isolated building. The floor stiffness, floor mass, floor viscous damping coefficient and parameters of the bilinear model of the isolation system are illustrated in Fig. 2. In their investigation, the behavior of the base isolation system is considered to be a bilinear hysteresis model, and the superstructure is considered to be linear–elastic during the numerical analysis. The output result of their investigation is illustrated in Fig. 3b.

Moreover, Kulkarni et al. [20] investigated a five-story base-isolated building with one degree of freedom at each floor. In their study, the behavior of the force–deformation of the laminated rubber bearing (LRB) is considered to be equivalent linear, and the LCRB or NZ is considered to be bilinear. Finally, the results related to the top floor acceleration and the base displacements are shown in Table 1 (mid-column of Table 1 related to Ref [20]).

In the aforementioned studies, numerical analysis was implemented using Newmark's step-by-step method of integration.

Based on the above studies, for the purpose of verification, parameters were extracted from previous studies (data illustrated both in Fig. 2 [17] and Table 1 [20]) and then implemented into the program, which is written in MATLAB, for modeling. In the present study, the solutions of equations are performed using the Runge–Kutta method, which is known as an implicit and explicit iterative method. The similarity between the results illustrated in Fig. 3 and Table 1 confirms the validity of the program.

3 Numerical Study

In this study, the lumped-mass stick model, which has been introduced by Kelly [21, 22], is used to represent a multi-degree of freedom structure (Fig. 4c). The modeling and time-history analyses of the subjected isolated buildings are carried out using MATLAB.

3.1 Structural Parameters

The subject base-isolated buildings are considered symmetrical square buildings consisting of six bays in each direction and have been modeled as a shear type steel structure mounted on isolation systems with one lateral degree of freedom at each floor (Fig. 4). The floors are in alignment and equal in height, which is considered to be $h = 3$ m each. In this study, as the investigated buildings are represented as residential area—category "A" [23], the live load uniformly

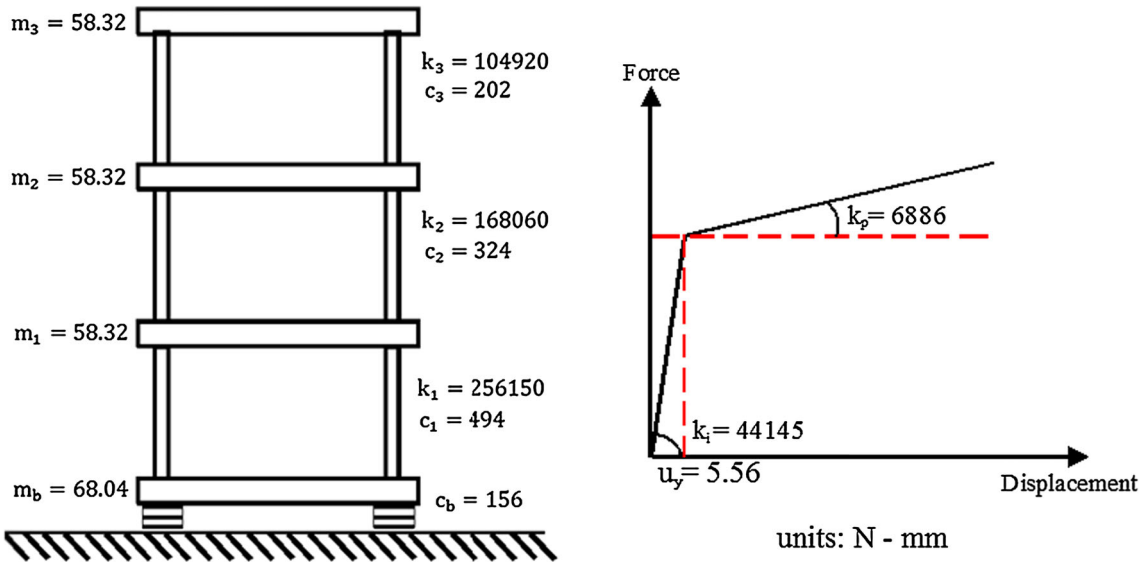

Fig. 2 Model parameters of the 3-story base-isolated building [17] (the stiffness is in N/mm, damping coefficient is in Ns/mm, and mass is in tons)

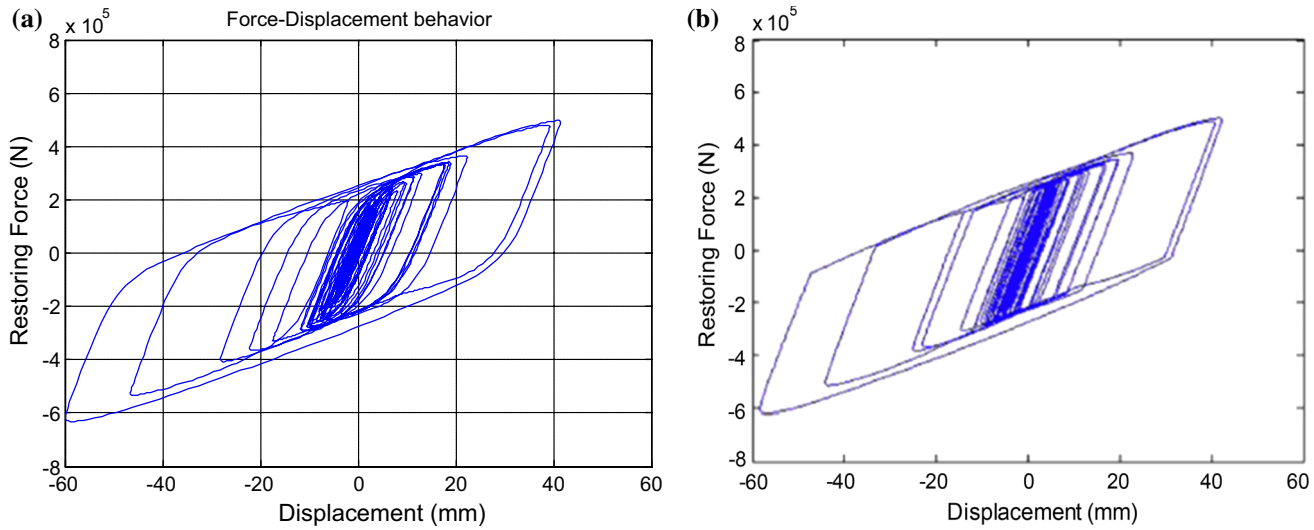

Fig. 3 LCRB numerical analysis model validation with the results of [17]: **a** validated and **b** the results given in Ref [17]

distributed in the amount of 1500 N/m^2. According to the Eurocode, the live loads (LLs) are reduced, with a factor of $\psi_{2i} = 0.3$ in a seismic design situation [24]. In addition, uniform surface loads (dead loads or DLs) have been considered to be 260 0 N/m^2. By adding the loads (DL + ψ_{2i}LL), the total loads were calculated to be 3053.2 N/m^2.

As the story dimension of the subjected building is 30 m × 30 m (Fig. 4d), the mass for each story is calculated to be 2.748×10^5 kg. Since the plan of the building is symmetric, frame 4 has been selected as a representative to study the behavior of the subjected buildings. According to the loaded area, the mass calculated for frame 4 is 45,798.3 kg.

During analysis, the following assumptions are made for the subjected structural systems:

- Throughout the time-history analyses, the superstructure is assumed to remain linear–elastic
- The force–deformation behavior of the LCRB is considered to be bilinear, modeled by Wen's equation [16]
- Each floor is considered to be rigid in its own plane
- No overturning over the base isolation system will occur during the sliding

In this investigation, **M** is the diagonal mass matrix, which is defined by the mass of each floor for the superstructure and kept constant (i.e., $m_i = m, i = 1, 2, \ldots, N$). Moreover, the base mass of the isolated building (m_b) is considered to be equal to the floor mass ($m_b = m$). The modal damping ratio of the steel buildings remained unchanged for all modes (ξ_s)

Table 1 Numerical analysis model validation with the results given in Ref [20]

Ts	Numerical analysis				Results in [20]				Difference in percent (%)			
	Top floor Abs Acc. (g)		Base Dis. (cm)		Top floor Abs Acc. (g)		Base Dis. (cm)		Acc. ratio	Acc. ratio	Dis. ratio	Dis. ratio
	LRB	NZ (LCRB)	LRB	NZ (LCRB)	LRB	NZ (LCRB)	LRB	NZ (LCRB)	LRB (%)	NZ (LCRB) (%)	LRB (%)	NZ (LCRB) (%)
0.4	0.358	0.3714	31.59	28.2	0.358	0.376	31.5	29.3	0.06	2.02	0.93	3.75
0.5	0.432	0.426	30.91	27.9	0.427	0.4239	30.57	28.7	1.13	0.72	1.01	2.787
0.6	0.476	0.4224	29.86	27.31	0.473	0.4508	29	28	0.48	2.88	1.91	2.46
0.7	0.5	0.513	28.66	27.33	0.493	0.526	28	27.5	1.35	2.60	1.27	0.61
0.8	0.455	0.487	28.11	27.29	0.448	0.483	27.9	27.2	1.43	1.29	2.22	0.47

Acc. acceleration, *Dis.* displacement, *Abs.* absolute

and was set at 2%. The stiffness of each story (k) is taken in the proportions of 1, 1.5, 2, 2.5 and 3 (Table 2). The value of k can be computed by providing the required fundamental period of the fixed-base buildings as T_s. In this paper, the superstructure time period is defined as $T_s = 0.1$ N, where N is the number of stories of the superstructure above the isolation level [13, 14]. The story numbers for the buildings are selected as 5, 10, 15, 20, 25, 30 and 35 (Fig. 4a, b), thus considering the superstructure periods $T_s = 0.5$ s; 1.0 s; 1.5 s; 2.0 s; 2.5 s; 3.0 s and 3.5 s, respectively. Tables 2 and 3 illustrate the properties of the subject buildings and the period of vibration for the first five modes of the isolated buildings, respectively.

3.2 Base Isolation System Properties and Earthquake Components

In this study, the earthquake motions are selected randomly according to three different ratios, which are shown in Table 4 with their specifications. The top and bearing behavior of the isolated building is the response quantities of interest.

The behavior of the isolator is taken into account by choosing the acceptable values of the isolator's period adequate to $T_b = 2.5$ s, damping ratio $\xi_b = 5\%$, yielding displacement $u_y = 0.025$ m and the ratio of post-yielding stiffness to pre-yielding stiffness $\alpha_1 = 0.3$. Table 5 summarizes the information on the properties of the base isolation system and the base-isolated buildings (BIB) considered in this investigation.

In this study, to research the probabilistic performance evolution of the base-isolated buildings, a two-factor factorial design was conducted using Minitab software (version 2017), considering the factors (ratio of PGA/PGV and number of stories) in Table 6, while all other factors such as T_b, ξ_b, f_0, α_1 and u_y remained constant (Table 5). In Table 6, y_{abn} (i.e., y_{111}, y_{112}, …) is the result of the combination of a (ratio of PGA/PGV) and b (number of story) levels for nth ground motion.

For each group of earthquakes (for each ratio of PGA/PGV), 7 different kinds of buildings varying in height (i.e., 5, 10, 15, 20, 25, 30 and 35, as shown in Fig. 4a, b) have been considered, and combinations thereof are generated. Thus, there are 15 ground motions for each base-isolated building in each group of ground motions. Therefore, a total of 315 time-history analyses were carried out.

The ratio of PGA/PGV was mentioned as a very important factor affecting the behavior of the isolator. The behavior of the isolator can be reversed under various ground motions even for the same level acceleration of the earthquakes. The following figures (Fig. 5) illustrate the spectral acceleration for each group of earthquakes along with their median, which makes it easy to clarify the difference between the groups of the earthquakes. The acceleration spectra of the

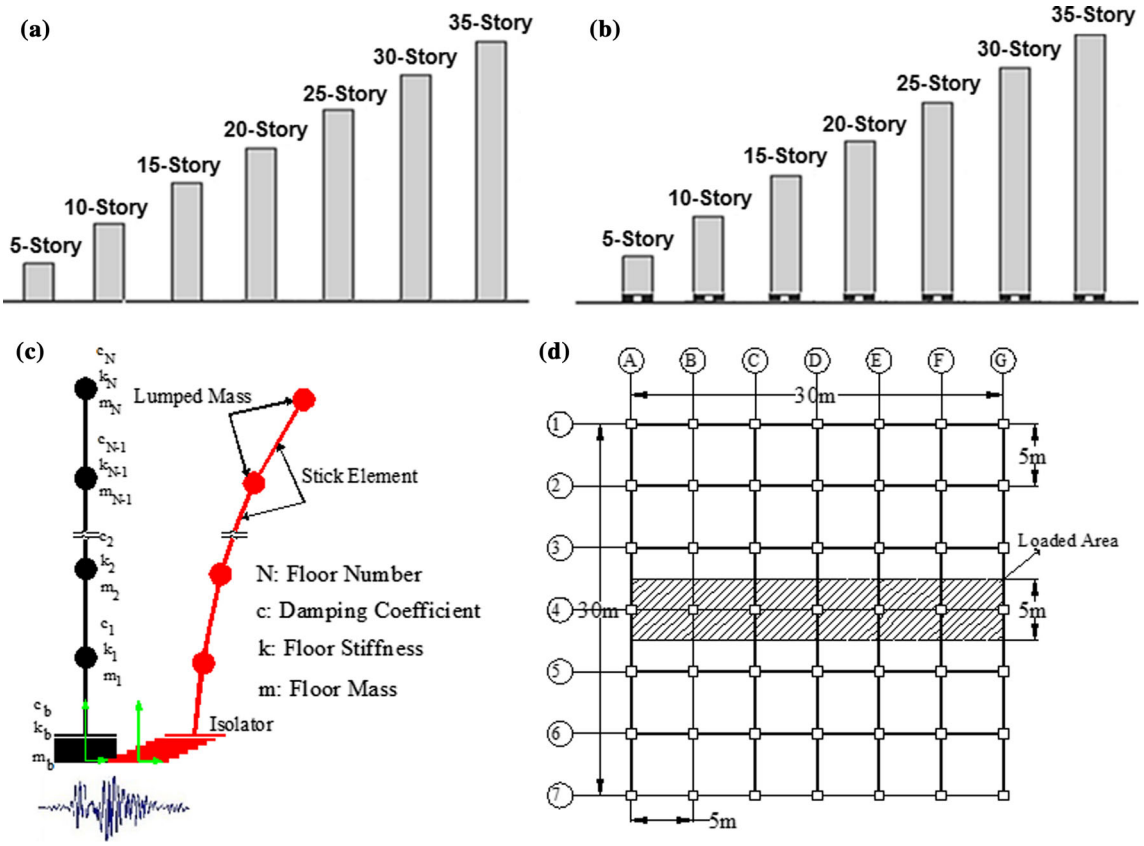

Fig. 4 Subject buildings: **a** fixed-base building (FBB); **b** base-isolated building (BIB); **c** lumped-mass stick model; and **d** area plan and selected frame with loaded area

Table 2 Stiffness proportion and mass properties of the subjected superstructures (steel buildings)

	5-Story	10-Story	15-Story	20-Story	25-Story	30-Story	35-Story	Stiffness proportion	m (mass for frame 4 in kg)	ξ_s (%)
Floor level	1	1–2	1–3	1–4	1–5	1–6	1–7	k	45,798.3	2
	2	3–4	4–6	5–8	6–10	7–12	8–14	$k/1.5$	45,798.3	
	3	5–6	7–9	9–12	11–15	12–18	15–21	$k/2$	45,798.3	
	4	7–8	10–12	13–16	16–20	19–24	22–28	$k/2.5$	45,798.3	
	5	9–10	13–15	17–20	21–25	25–30	29–35	$k/3$	45,798.3	

Table 3 Period of vibration for each mode of isolated buildings and nonisolated buildings

Mode	Period of vibration (s)													
	5-Story		10-Story		15-Story		20-Story		25-Story		30-Story		35-Story	
	BIB	FBB	BIB	FBB	BIB	FBB	BIB	FBB	BIB	FBB	BIB	FBB	BIB	FBB
1	2.51	0.50	2.64	1.00	2.83	1.50	3.08	2.00	3.40	2.50	3.76	3.00	4.16	3.50
2	0.31	0.18	0.60	0.37	0.82	0.55	1.03	0.73	1.22	0.92	1.39	1.10	1.56	1.28
3	0.16	0.12	0.30	0.22	0.43	0.33	0.56	0.45	0.68	0.56	0.81	0.67	0.92	0.78
4	0.12	0.09	0.20	0.16	0.29	0.24	0.38	0.32	0.47	0.40	0.56	0.48	0.64	0.56
5	0.09	0.07	0.16	0.13	0.22	0.19	0.29	0.25	0.36	0.31	0.43	0.37	0.49	0.43

Table 4 Ground motions for different cases of *PGA/PGV*

No.	EQ. ID	Earthquake name	Year	Duration time (EQ.)	PGA (g)	PGV (m/s)	PGD (m)	PGA/PGV	
1	25	"TCGH13"	2004	21	0.590	0.626	0.098	0.945	PGA/PGV < 1
2	7	"KOBE, Japan"	1995	50	0.834	0.911	0.211	0.915	
3	2	"Imperial Valley-02"	1940	55	0.280	0.309	0.087	0.905	
4	10	"Tabas_ Iran"	1978	40	0.027	0.034	0.031	0.768	
5	29	"Tabas, Iran"	1978	33	0.861	1.234	0.936	0.698	
6	22	"Bam_ Iran"	2003	33	0.014	0.020	0.013	0.696	
7	3	"Imperial Valley-02"	1940	55	0.210	0.313	0.241	0.670	
8	17	"El Mayor-Cucapah_ Mexico"	2010	130	0.248	0.383	0.482	0.648	
9	30	"Northridge-01"	1994	28	0.426	0.748	0.190	0.569	
10	8	"Kocaeli_ Turkey"	1999	150	0.045	0.081	0.035	0.555	
11	23	"Tottori, Japan"	2000	120	0.018	0.036	0.042	0.511	
12	19	"Duzce_ Turkey"	1999	95	0.017	0.045	0.038	0.373	
13	28	"Northridge-01"	1994	30	0.410	1.114	0.446	0.368	
14	14	"Darfield_ New Zealand"	2010	140	0.194	0.591	0.491	0.328	
15	20	"Darfield_ New Zealand"	2010	120	0.209	0.671	0.599	0.311	
1	33	"Loma Prieta"	1989	40	0.416	0.208	0.061	1.997	1 < PGA/PGV < 2
2	31	"Parkfield"	1966	30	0.272	0.154	0.031	1.770	
3	16	"Ierissos Greece"	1983	18	0.030	0.017	0.002	1.737	
4	15	"Friuli_ Italy 01"	1976	40	0.069	0.040	0.005	1.717	
5	34	"Tottori, Japan"	2000	300	0.337	0.197	0.064	1.704	
6	1	"Imperial Valley-05"	1955	40	0.050	0.037	0.009	1.361	
7	9	"Duzce_ Turkey"	1999	60	0.734	0.559	0.255	1.312	
8	5	"Imperial Valley-06"	1979	38	0.598	0.467	0.202	1.279	
9	21	"Friuli_ Italy 01"	1976	17	0.029	0.023	0.012	1.252	
10	18	"Duzce_ Turkey"	1999	58	0.806	0.658	0.130	1.223	
11	32	"Irpinia, Italy 01"	1980	25	0.034	0.030	0.005	1.140	
12	11	"Bam_ Iran"	2003	45	0.032	0.028	0.027	1.130	
13	35	"Tottori, Japan"	2000	135	0.131	0.116	0.041	1.125	
14	4	"Imperial Valley-03"	1951	40	0.030	0.027	0.004	1.125	
15	27	"Shin-Osaka"	1995	40	0.233	0.218	0.097	1.069	
1	13	"Tottori, Japan"	2000	300	0.410	0.088	0.025	4.661	PGA/PGV > 2
2	41	"Westmorland"	1981	30	0.232	0.054	0.009	4.240	
3	37	"San Fernando"	1971	35	0.169	0.047	0.011	3.571	
4	6	"Imperial Valley-07"	1979	18	0.118	0.036	0.003	3.269	
5	38	"Fruili, Italy 03"	1976	15	0.112	0.038	0.002	2.893	
6	40	"Livermore-02"	1980	40	0.254	0.098	0.005	2.590	
7	43	"Nahanni, Canada"	1985	11	1.107	0.439	0.068	2.522	
8	36	"Parkfield"	1966	25	0.271	0.113	0.038	2.392	
9	12	"9173365"	2001	120	0.010	0.004	0.00044	2.381	
10	45	"Tottori, Japan"	2000	300	0.289	0.124	0.043	2.327	
11	26	"Whittier Narrows-01"	1987	50	0.121	0.052	0.007	2.323	
12	39	"Coyote Lake"	1979	28	0.094	0.042	0.008	2.226	
13	24	"Dinar Turkey"	1995	29	0.065	0.031	0.002	2.101	
14	44	"Loma Prieta"	1989	40	0.460	0.227	0.081	2.022	
15	42	"Coalinga-05"	1983	20	0.405	0.201	0.014	2.012	

Table 5 Properties of the base isolation system and base-isolated buildings (BIBs)

No. story	5	10	15	20	25	30	35
T_b (s)	2.5	2.5	2.5	2.5	2.5	2.5	2.5
k_b (N/m)	1.74e6	3.18e6	4.63e6	6.075e6	7.52e6	8.97e6	10.41e6
k_i (N/m)	5.78e6	10.60e6	15.43e6	20.25e6	25.07e6	29.90e6	34.71e6
ξ_b (%)	5	5	5	5	5	5	5
α_1	0.3	0.3	0.3	0.3	0.3	0.3	0.3
u_y (m)	0.025	0.025	0.025	0.025	0.025	0.025	0.025
$f_0 = \frac{Q}{W}$	0.05	0.05	0.05	0.05	0.05	0.05	0.05
m_b (base mass) kg	45,798.3	45,798.3	45,798.3	45,798.3	45,798.3	45,798.3	45,798.3
First-mode period (s)	2.51	2.64	2.83	3.08	3.40	3.76	4.16
Third-mode period (s)	0.16	0.30	0.43	0.56	0.68	0.81	0.92

Table 6 Arrangement for two-factor factorial design

Factor	Levels	Stories						
		5	10	15	20	25	30	35
Ratio	1 > PGA/PGV	y_{111}	y_{121}	y_{131}	y_{141}	y_{151}	y_{161}	y_{171}
		y_{112}	y_{122}	y_{132}	y_{142}	y_{152}	y_{162}	y_{172}
		⋮	⋮	⋮	⋮	⋮	⋮	⋮
		y_{11n}	y_{12n}	y_{13n}	y_{14n}	y_{15n}	y_{16n}	y_{17n}
	1 < PGA/PGV < 2	y_{211}	y_{221}	y_{231}	y_{241}	y_{251}	y_{261}	y_{271}
		y_{212}	y_{222}	y_{232}	y_{242}	y_{252}	y_{262}	y_{272}
		⋮	⋮	⋮	⋮	⋮	⋮	⋮
		y_{21n}	y_{22n}	y_{23n}	y_{24n}	y_{25n}	y_{26n}	y_{27n}
	PGA/PGV > 2	y_{311}	y_{321}	y_{331}	y_{341}	y_{351}	y_{361}	y_{371}
		y_{312}	y_{322}	y_{332}	y_{342}	y_{352}	y_{362}	y_{372}
		⋮	⋮	⋮	⋮	⋮	⋮	⋮
		y_{31n}	y_{32n}	y_{33n}	y_{34n}	y_{35n}	y_{36n}	y_{37n}

selected ground motions in Fig. 5 illustrate that as the ratio of PGA/PGV increases, by shifting the period to 2.5 s, their spectral accelerations decrease (at 2.5 s).

4 Results and Discussion

4.1 Probabilistic Behavior Evaluation of the Base Isolation Systems and Base-Isolated Buildings

With regard to Fig. 6a, when PGA/PGV $<$ 1, the ratio of isolator displacement to peak ground displacement (PGD) is approximately 0.64, and as it changes to 1 $<$ PGA/PGV $<$ 2 and further to PGA/PGV $>$ 2, the ratio increases. The graph also shows that the case of 1 $<$ PGA/PGV $<$ 2 is the mean of the other two cases (i.e., PGA/PGV $<$ 1 and PGA/PGV $>$ 2).

Moreover, with regard to the number of stories in the base-isolated buildings (Fig. 6b), it can be clarified that by increasing the number of stories, marginal changes are observed between 5- and 10-story buildings, and the ratio gradually decreases, which is not significant. In addition, the ratio is at the highest level for the 5- and 10-story buildings, which implies that the isolator displacement with respect to the peak ground displacement increases by approximately 0.1. For the case of the 20-story building, the ratio of isolator displacement to peak ground displacement is sharply decreased, which can be the result of the flexibility of the high-rise building and its effect on the base isolation system.

Additionally, the interaction of both the PGA/PGV ratio and the effects of the number of stories show that the trend is quite similar for all types of base-isolated buildings, and the ratio increases. The ratio of isolator displacement to peak ground displacement (ISO DIS TO PGD) for the cases when PGA/PGV $<$ 1 is the lowest and for the case when PGA/PGV $>$ 2 is the highest is shown in Fig. 6c. In addition, as the number of stories increases, the ratio decreases, which can also be the result of the flexibility of the high-rise buildings.

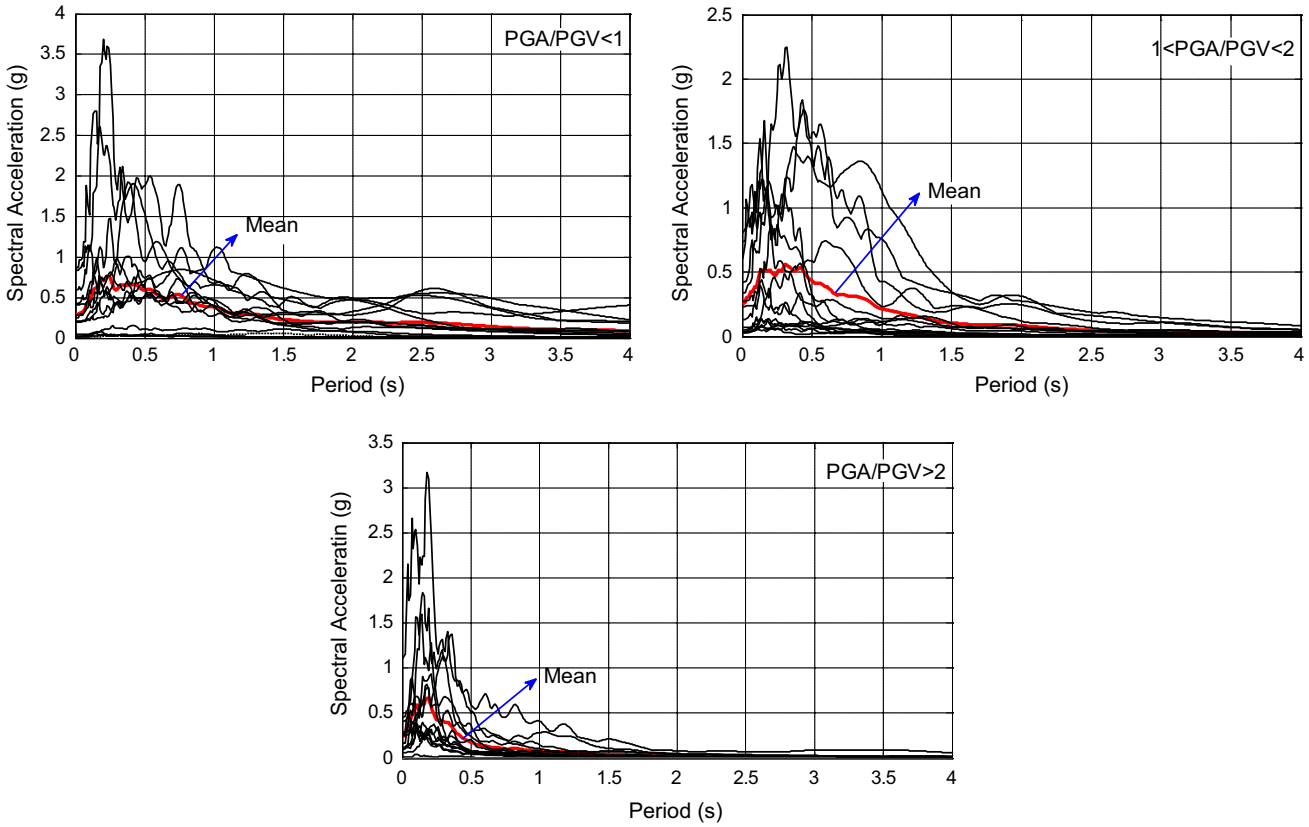

Fig. 5 Five percent (5%) damped acceleration spectra of the selected ground motions for three cases

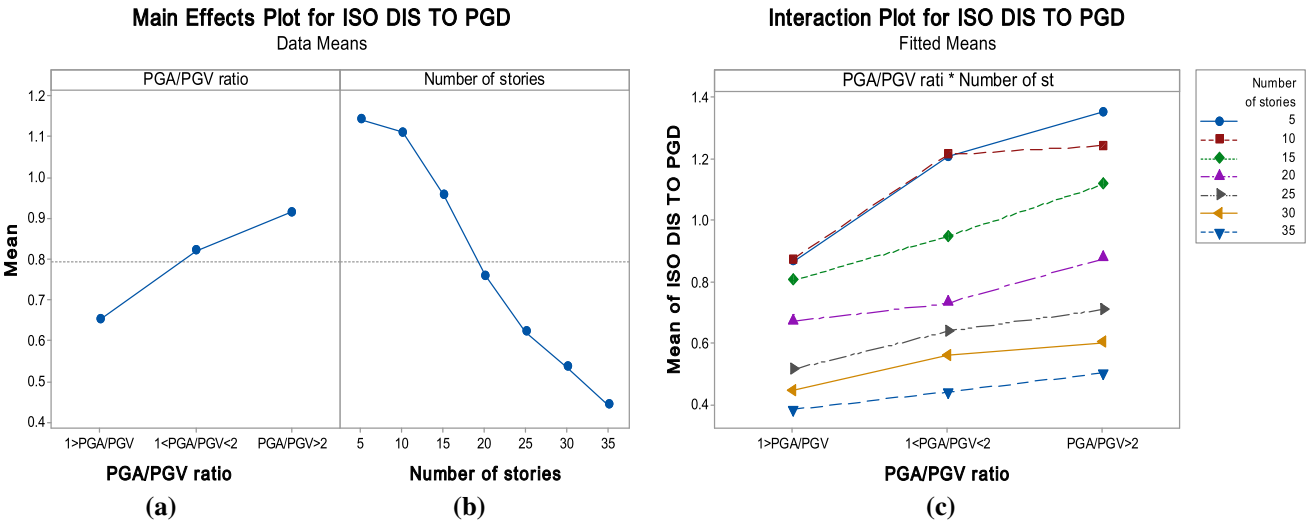

Fig. 6 Main effects and interaction plots for isolator displacement with respect to PGD

Additionally, Fig. 7a shows that the ratio of the top floor displacement to the peak ground displacement (ROOF DIS TO PGD) has been significantly increased for the cases between $1 < \text{PGA/PGV} < 2$ and $\text{PGA/PGV} < 1$ and remained almost constant between the cases $1 < \text{PGA/PGV} < 2$ and $\text{PGA/PGV} > 2$. Moreover, as the ratio of PGA/PGV is more than one, it implies that the displacement for the top floor is highly increased with respect to the peak ground displacement. In addition, in Fig. 7b, it can be observed that by increasing the number of stories, the ratio of top floor displacement to peak ground displacement is increased, which is also expected as the height of the building increases. Only the 5 and 10 story buildings have a ratio lower than 1.

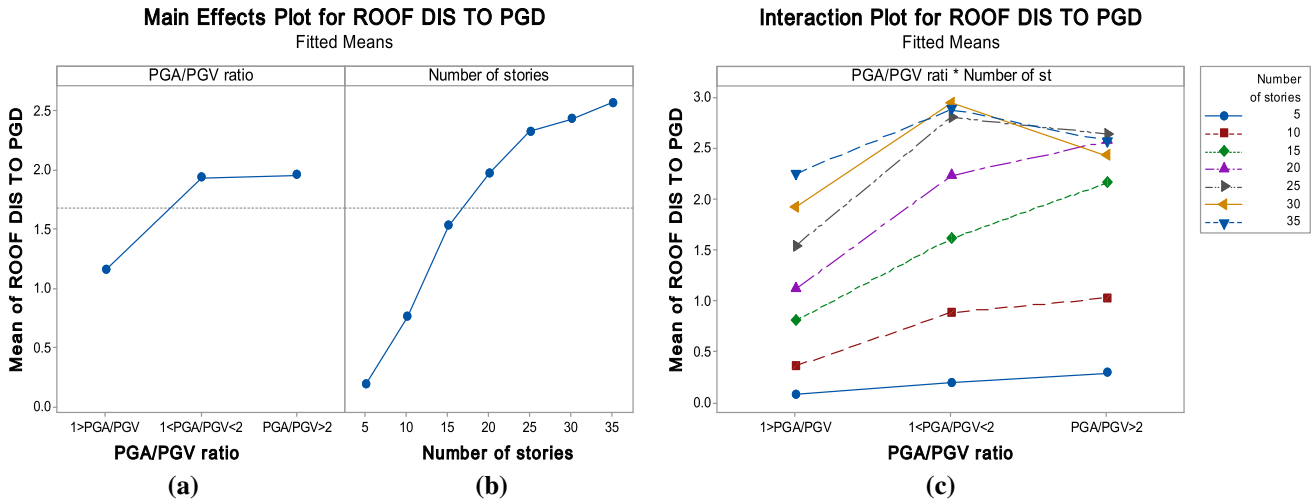

Fig. 7 Main effects and interaction plots for roof displacement with respect to PGD

Figure 7c, which is the interaction plot, shows that the ratios for 5-, 10-, 15- and 20-story buildings increase with the same trend, which also shows that there is no interaction; however, for 25-, 30- and 35-story isolated buildings, the ratio increased for the case when $1 < \text{PGA/PGV} < 2$ and decreased for the case when $\text{PGA/PGV} > 2$. Moreover, the ratio of roof displacement to PGD decreased for 5- and 10-story buildings for the three cases (see Table 4). However, for a 15-story building, roof displacement decreased only in the case when $\text{PGA/PGV} < 1$. In contrast, for the 20-, 25-, 30- and 35-story buildings, roof displacement increased with respect to PGD, which implies that the displacement is higher than the ground displacement.

Figure 8a gives information about the ratio of the isolator acceleration to peak ground acceleration (ISO ACC TO PGA), where this ratio is highly increased for the case of ground motions with $\text{PGA/PGV} < 1$ when compared with the other two cases of $1 < \text{PGA/PGV} < 2$ and $\text{PGA/PGV} > 2$. However, overall, the acceleration is not more than the ground acceleration for three different cases.

Moreover, Fig. 8b shows that because the number of stories increases, the isolator acceleration with respect to PGA fluctuates. It can be concluded that for different heights and stories, the acceleration of the isolation system in base-isolated buildings will be reduced by approximately 55% with respect to the PGA.

By observing the interaction (Fig. 8c) of the ratio of PGA/PGV and the number of stories, it is clear that unlike the displacement ratio mentioned above, the proportion of isolator acceleration to peak ground acceleration (PGA) for all isolated buildings decreases in a similar trend as the ratio of PGA/PGV increases. In all cases, the base isolation acceleration is decreased with respect to the peak ground acceleration. Furthermore, increasing the number of stories has no signif-

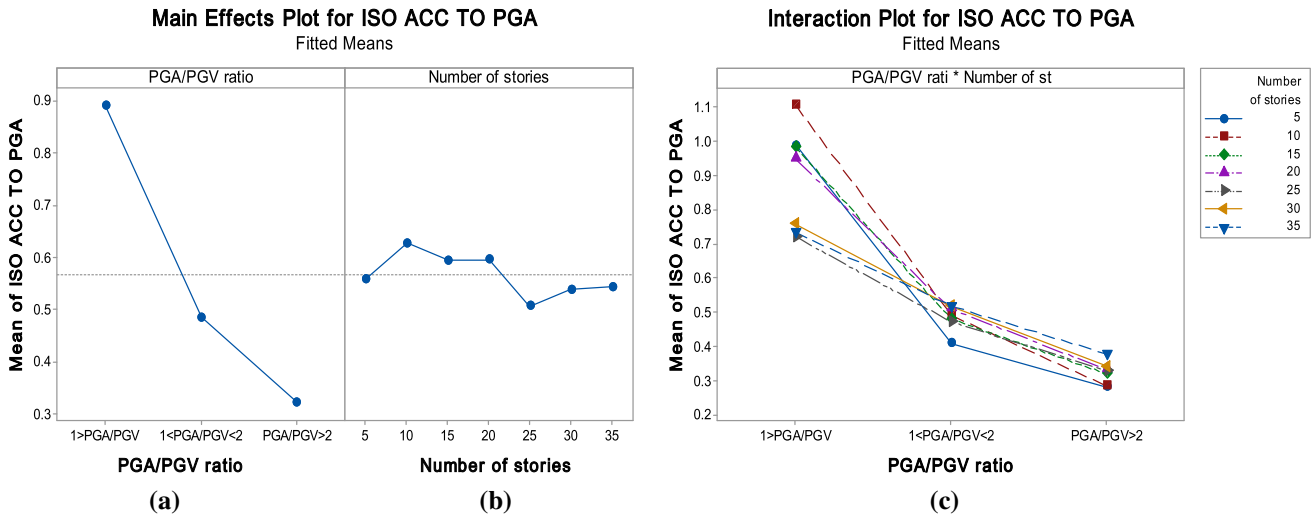

Fig. 8 Main effects and interaction plots for isolator acceleration with respect to PGA

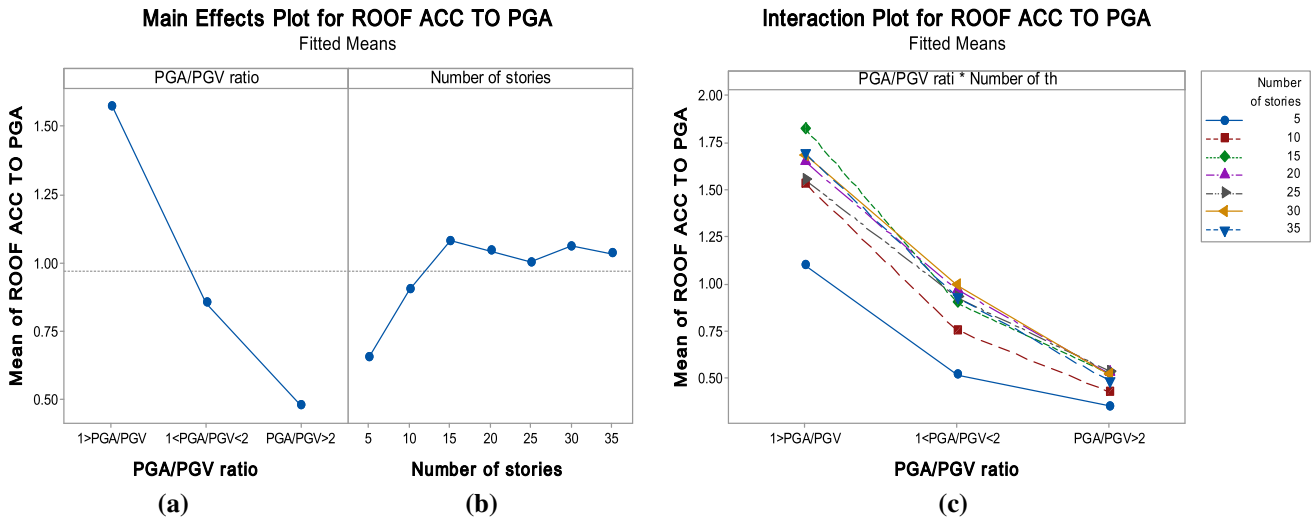

Fig. 9 Main effects and interaction plots for roof acceleration with respect to PGA

icant effect for the cases when $1 < \mathrm{PGA/PGV} < 2$ and $\mathrm{PGA/PGV} > 2$, and the ratios calculated are closer to each other for all types of buildings in the stated cases (Fig. 8c).

Figure 9a shows that when $\mathrm{PGA/PGV} < 1$, roof acceleration is further increased compared to the cases when $1 < \mathrm{PGA/PGV} < 2$ and $\mathrm{PGA/PGV} > 2$, which is approximately 1.75 times higher than the PGA. In addition, Fig. 9b illustrates that roof acceleration is decreased for 5- and 10-story buildings with reference to the PGA (i.e., roof acceleration is lower than the PGA), but this ratio is higher than one for five other different buildings (i.e., roof acceleration is higher than the PGA), and it also fluctuates because the number of stories increases. In addition, considering the interaction plot (Fig. 9c), it can be seen that for all types of isolated buildings, the ratio for the case when $\mathrm{PGA/PGV} < 1$ is more than that of the cases when $1 < \mathrm{PGA/PGV} < 2$ and $\mathrm{PGA/PGV} > 2$, and the roof acceleration is more than the PGA. This ratio is decreased for the cases of $1 < \mathrm{PGA/PGV} < 2$ and $\mathrm{PGA/PGV} > 2$, which shows that the ratio is less than one and roof acceleration is lower than the peak ground acceleration in these two cases. Additionally, the ratios for the case when $\mathrm{PGA/PGV} > 2$ are closer to each other for all types of buildings (Fig. 9c).

4.2 Performance of the Base Isolation System and Base-Isolated Building

As shown in Fig. 10, the fundamental period of the base-isolated building increases as the number of stories increases, which implies that the influence of the base isolation system decreases as the number of stories or the flexibility of the superstructure increases. The figure also shows that as the number of stories increases, the gap between the fundamental period of the fixed-base building and the base-isolated building decreases. It also seems that as this trend continues, there is no difference between the fixed-base and base-isolated buildings' fundamental periods, and thus, the effect of the base isolation system is reduced.

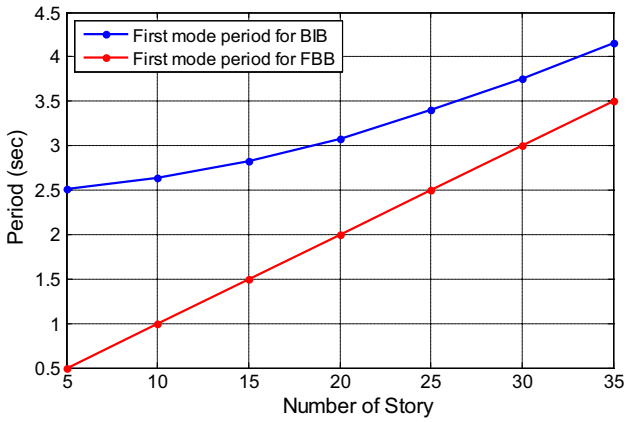

Fig. 10 Fundamental period of the superstructure for both fixed-base and base-isolated systems (when the base isolation period is $T_b = 2.5$ s)

The figure clearly shows that as the fundamental period of the 5-story fixed-base building is approximately 0.5 s, if an isolation system is mounted on this building, the fundamental period increases, which is approximately 5 times higher than that of the fixed base. However, this shift gradually decreases as the number of stories increases; for example, as the fundamental period of the 35-story fixed-base building is approximately 3.5 s, if an isolation system is mounted on this building, the fundamental period increases approximately 1.2 times when compared with the 35-story fixed-base building.

For further investigation, from each group of selected earthquakes, one earthquake with the highest PGA was

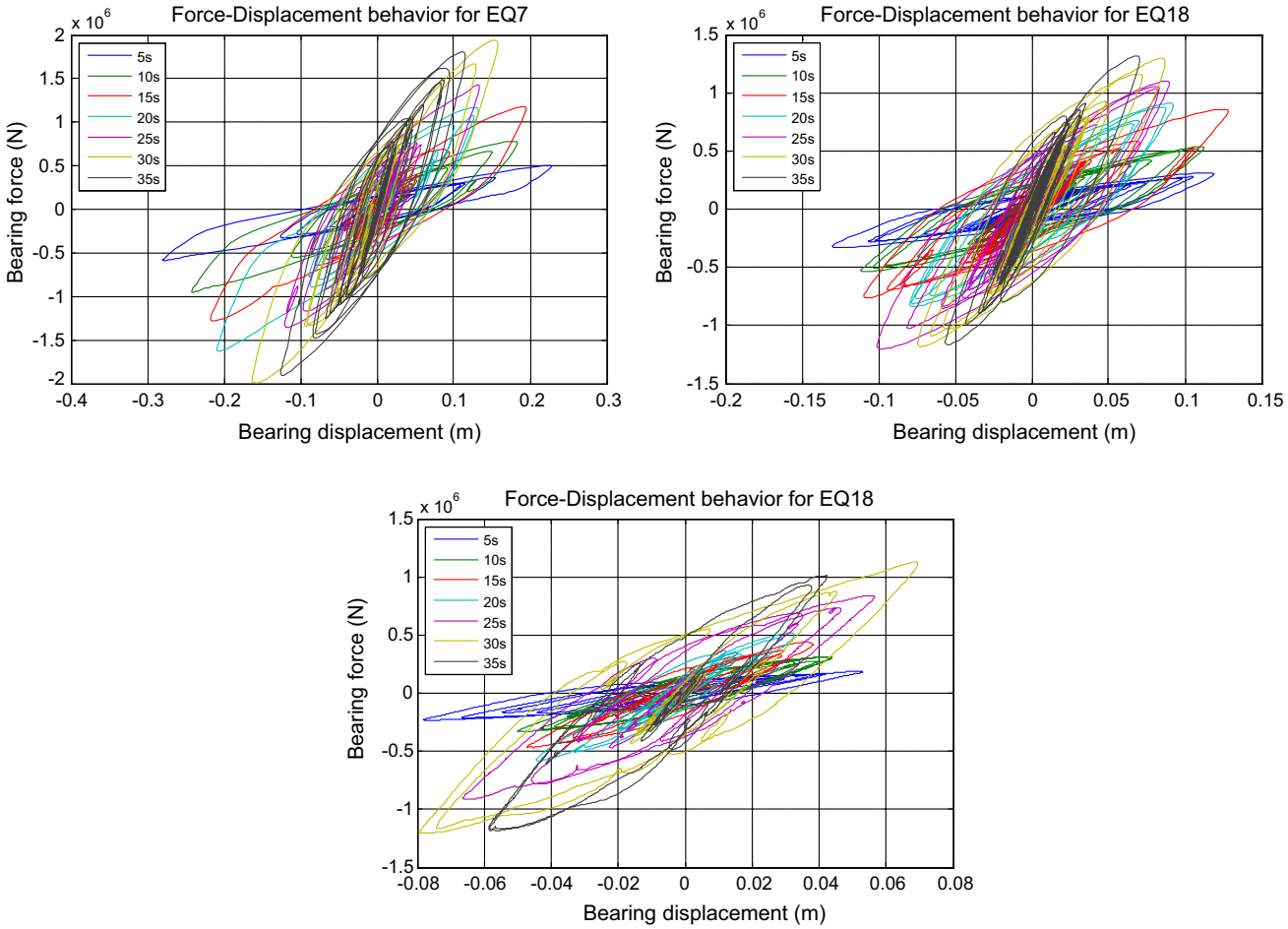

Fig. 11 Force–displacement curves for three selected ground motions with the highest PGA

selected to study the amount of dissipated energy as the number of stories increased. Figure 11 illustrates that as the number of stories is increased, the shear force increases; consequently, the amount of dissipated energy by the base isolation system increases simultaneously (i.e., the area under the load–deflection curve increases).

In addition, the force–displacement curves of the base isolation system for three different cases of ground motions with maximum PGAs have been investigated on seven different base-isolated buildings, and the results are illustrated in Fig. 12. As seen, less energy has been dissipated for the case when PGA/PGV $>$ 2. Based on Fig. 5, according to the characteristics of earthquakes, by shifting the period to 2.5 s, the amount of spectral acceleration for the median is lower for the case of PGA/PGV $>$ 2 when compared with the other two cases. This states that when the base-isolated buildings are subjected to the earthquake of case 3, low earthquake impact loads are applied to the structure, and as a result, less energy is required to be dissipated. Conversely, for the other ground motions, the applied load to the buildings is higher for the cases when 1 $<$ PGA/PGV $<$ 2 and PGA/PGV $<$ 1. Thus, more energy is required to be dissipated. This result can be clearly seen from the area under the force–displacement curves.

Figures 13 and 14 illustrate the median responses of the subject buildings induced by three different cases of the selected ground motions (see Table 4). Figure 13 shows that the percentage of reduction in acceleration is higher than the displacement at the top of the buildings when compared with fixed-base buildings. This amount of acceleration reduction is higher for low-rise buildings, but this reduction percentage decreases as the number of stories increases, and it can even be seen that there is no difference between the fixed-base and base-isolated buildings for the case when PGA/PGV $>$ 2 for 30- and 35-story buildings. Moreover, the magnitude of reduced acceleration for 15-, 20-, 25-, 30- and 35-story buildings remains approximately constant for each case of ground motions (see Table 4).

Figure 14 shows that by increasing the number of stories, the magnitude of the top floor displacement varies for the fixed base for the three different cases. However, for the base-isolated buildings, by increasing the number of stories, the

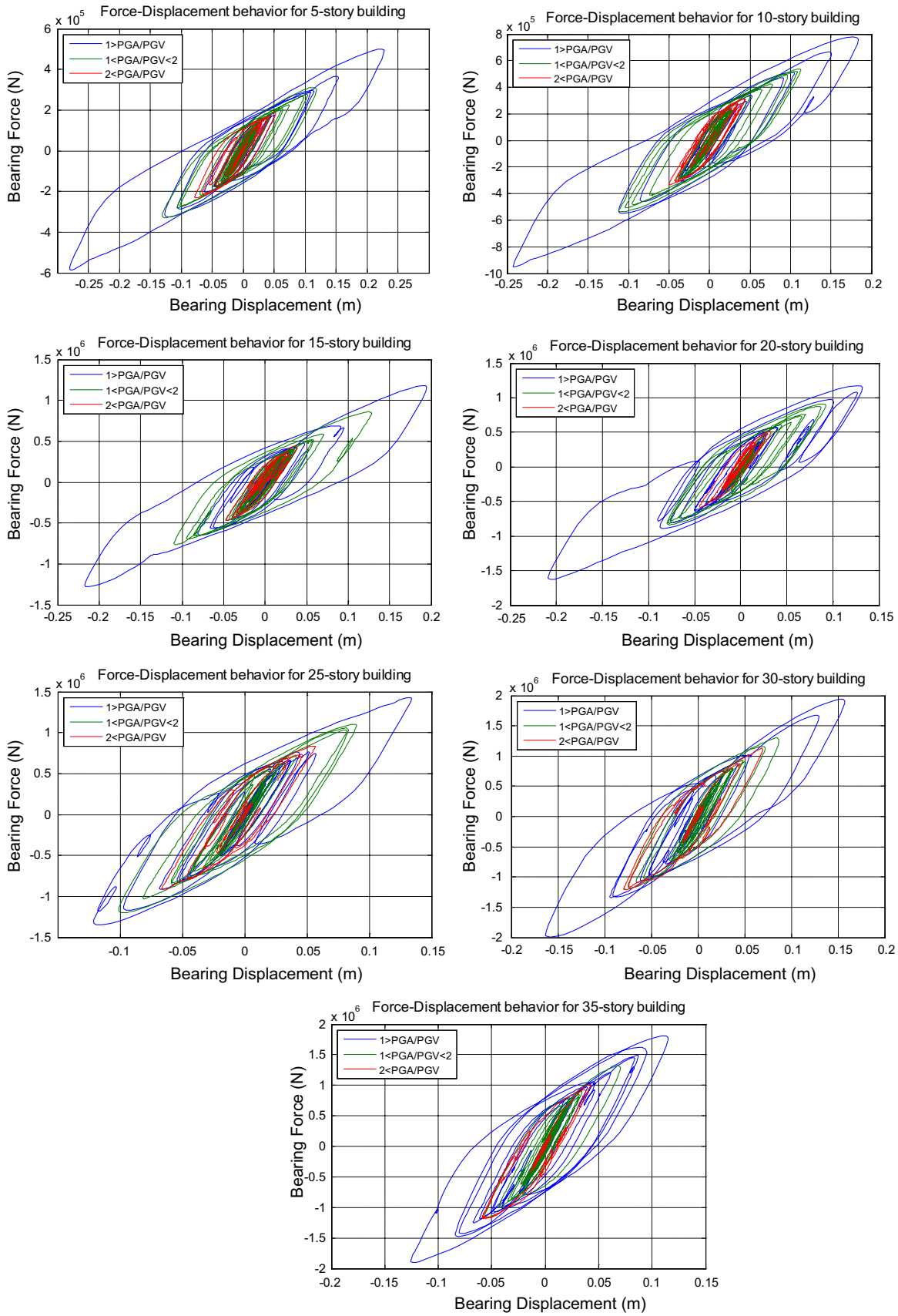

Fig. 12 Force–displacement behavior of the isolation system for seven different isolated buildings

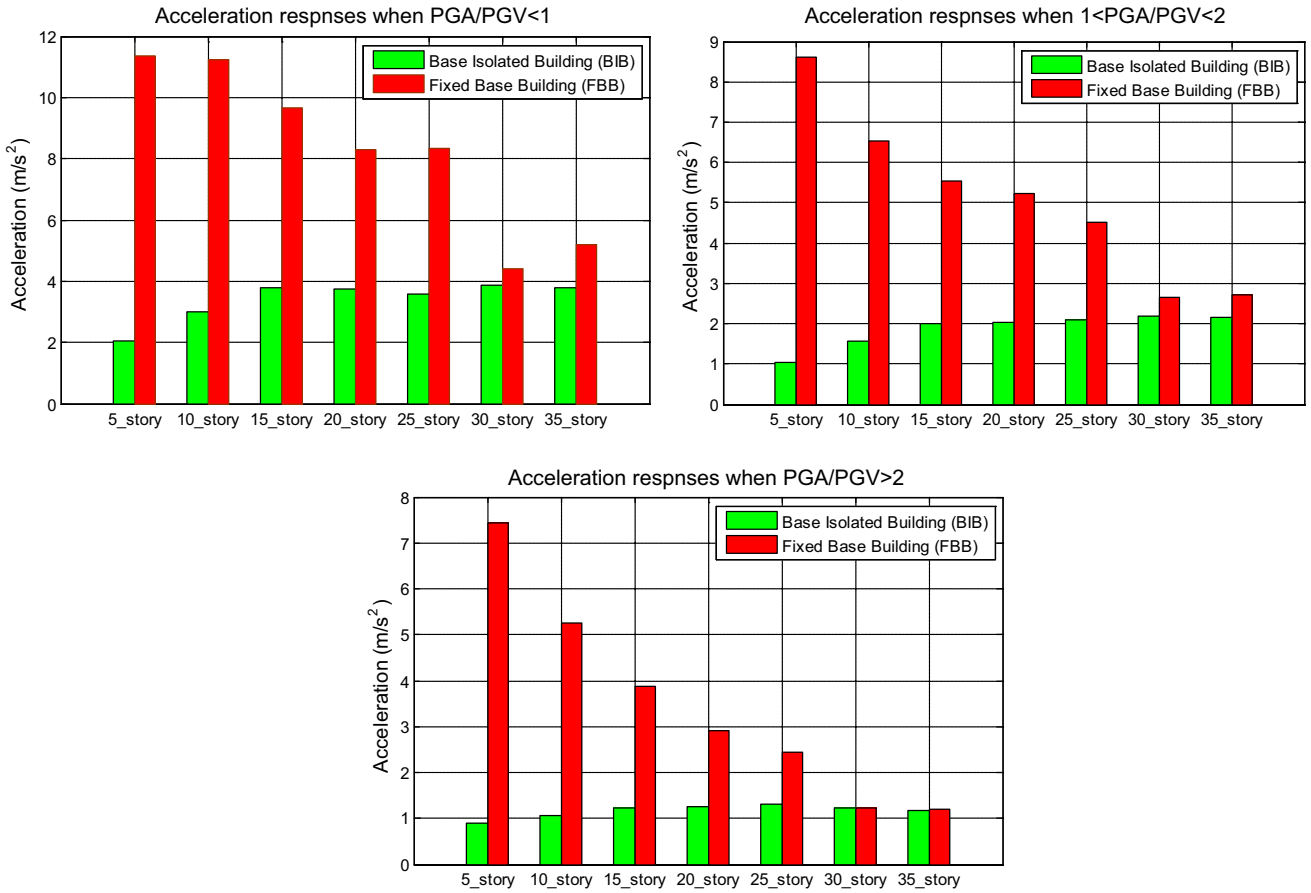

Fig. 13 Median of top floor absolute acceleration of the fixed-base and base-isolated buildings

top floor displacement of the buildings gradually increases. It is clear that the displacement has been decreased for the 5-, 10-, 15-, 20- and 25-story buildings but increases for 30- and 35-story buildings when compared with the fixed-base state, the results for which are inverse.

For further investigation, based on median spectrum ground motions in Fig. 5, artificial earthquakes were generated using the SeismoArtif software program (version 2018). In this manner, the Saragoni and Hart envelope curve method was implemented considering the following specifications [25] (Fig. 15).

For the above-mentioned method, three parameters are needed to fully define the envelope shape; thus, in this study, these three parameters are kept as follows:

- Duration considered to be 20 s
- t_1 is kept at 4 s. This parameter should be a real number lower than the duration, which is the time instant corresponding to unitary intensity.
- Idur: This parameter should be a real number smaller than unity, which is the value of intensity corresponding to the last instant of time (default value amounts to 0.05).

By executing the aforementioned procedure, Fig. 16 shows that the actual spectrum matches the specific target spectrum with 5% damping (see Fig. 16).

According to the above implementation, artificial earthquakes have been generated based on the median spectrum of the natural ground motions for each case in Table 4 (Fig. 17a illustrates accelerograms that are generated with respect to the target spectrum for each case, and Fig. 17b shows the velocity time history based on the generated accelerogram). Table 7 depicts the peak ground responses of the artificial ground motions for three different cases (PGA/PGV). Figure 17 and Table 7 also show that for the case when PGA/PGV < 1, the intensity of the ground motion is higher when compared with the two other ratios.

Because of space limitations, the plots illustrate the results related to the base of the isolated buildings (bearing displacement and acceleration) for 5-, 20- and 35-story buildings that are subjected to the generated artificial earthquakes (Figs. 18, 19).

Figures 18, 19 and Table 8 show the bearing displacement and acceleration are mostly affected by the ground motions whose PGA/PGV < 1, which is where the responses are increased. Moreover, in Table 8, it can be observed

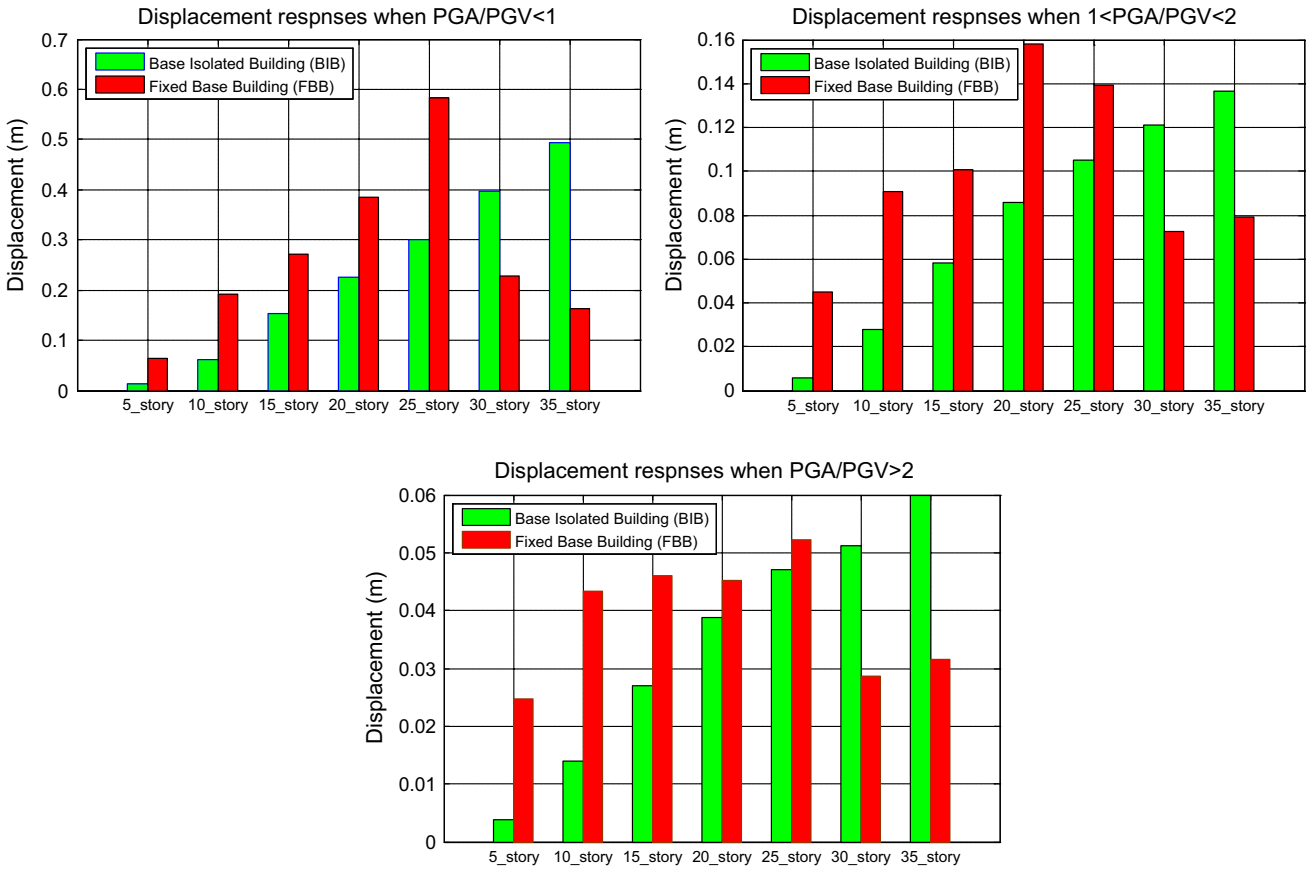

Fig. 14 Median of top floor relative displacement of the FB and BI buildings

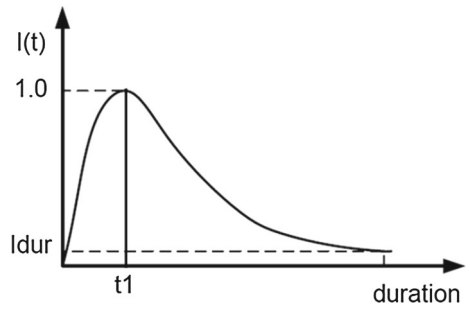

Fig. 15 Saragoni and Hart envelope curve [25]

that for high-rise base-isolated buildings (20- and 35-story buildings), there are no significant changes between cases 1 (PGA/PGV < 1) and 2 (1 < PGA/PGV < 2) for the peak acceleration of the bearing, while it is in the lowest intensity in case 3 (PGA/PGV > 2). In Table 8, for the peak bearing displacement, it can be seen that there are considerable changes between three cases, and as the ratio increases, displacement highly decreases. In addition, according to the accelerogram generated based on the target spectrum for each case of ground motions (see Fig. 17) and the bearing displacements achieved for these kinds of earthquakes (Fig. 19), it can be concluded that as the ratio of PGA/PGV decreases, the bearing displacement sharply increases for 35-story base-isolated building in the case when PGA/PGV is smaller than 1 (Fig. 19). An implication of this is the possibility that base-isolated high-rise buildings (i.e., 20-, 25-, 30- and 35-story) can be vulnerable to the ground motions when the ratio of PGA/PGV is smaller than 1.

4.3 Damage Limitation

4.3.1 Ground Motions Selected

According to Eurocode8 [26], the ground motion at a given point on the surface is represented by the elastic response spectrum. The form of the elastic response spectrum is taken for the no-collapse, and the damage limitation requirement is illustrated schematically in Fig. 20.

In Fig. 20, "S_e" is the elastic response spectrum; "T" is the vibration period for a single degree of freedom structure; "a_g" is the design acceleration of the ground type A; "S" is the soil factor of the ground type A; "η" is the factor of damping correction (η equals 1 for 5% viscous damping); "T_1" and "T_2" are the lower and upper limits of the spec-

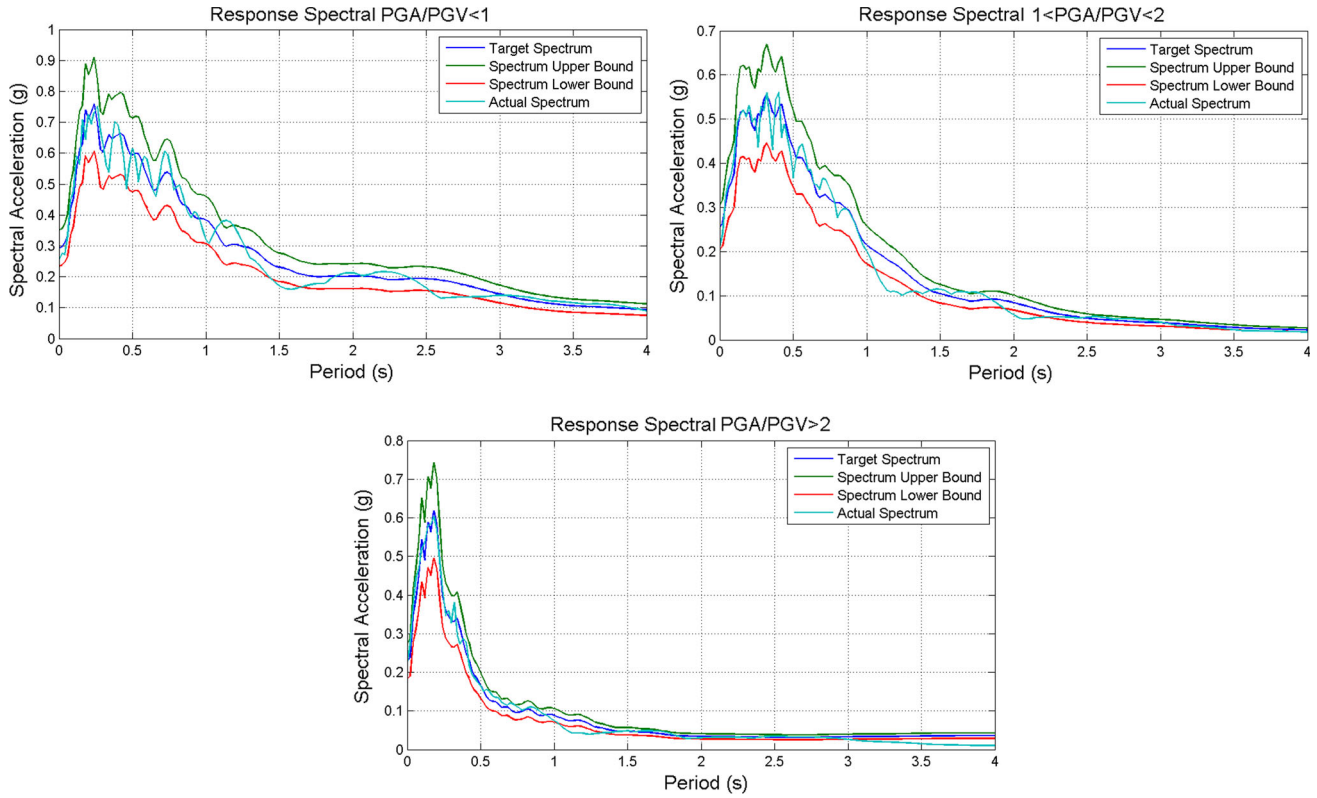

Fig. 16 Response spectral matched the target spectrum

tral acceleration branch, respectively; and "T_3" defines the beginning of the spectral acceleration.

By considering spectrum type 1 for ground type A, the reference peak ground acceleration for the case PGA/PGV < 1 results in $a_{gR} = 0.3g$ (Fig. 21). The form of the elastic response spectrum described by the value of soil factor (S) and the periods (T_1, T_2, T_3) results in $T_1 = 0.15$ s, $T_2 = 0.4$ s, $T_3 = 2.0$ s and $S = 1$ [26]. In the present paper, as the buildings are classified as importance class II, the corresponding importance factor is found to be $\gamma_1 = 1$ [24] (part 1, Table 4.3). Therefore, the peak ground acceleration equals the reference PGA, $a_g = \gamma_1 a_{gR}$. Using the equation in the code [26], the elastic response spectrum (ERS) can be shown for 5% damping, as shown in Fig. 21. Figure 21 depicts that the mean response spectrum of the subjected earthquakes for case 1 (PGA/PGV < 1) and the elastic response spectrum, which is the damage limitation requirement stated in the code, are compatible.

4.3.2 Drift Control

Accordingly, in this section, ground motions whose ratio of PGA/PGV is smaller than one have been implemented to study the damage limitation of the subjected buildings.

As the drift equals the deflection at one level minus the deflection below that level, the requirement of damage limitation should be considered in terms of the inter-story drift (d_r) [26], as follows:

$$d_r \nu \leq \alpha h \rightarrow \frac{d_r}{h} \leq \frac{\alpha}{\nu} \tag{13}$$

The drift of a story (d_r) is assessed as the difference in the average lateral displacements in the center of the mass at the top and bottom of the story (Fig. 22). The damage limitation is the requirement of the buildings at the upper limit on the inter-story drift ratio under seismic loading. The limit is set as [26]:

- if there are nonstructural elements in the building and forced to be stable under structural deformation, such as normal partitions ($\frac{d_r}{h} \leq \frac{0.005}{\nu}$)
- if there are nonstructural elements in the building that are ductile ($\frac{d_r}{h} \leq \frac{0.0075}{\nu}$)
- if there are no nonstructural elements in the buildings ($\frac{d_r}{h} \leq \frac{0.010}{\nu}$)

In Eq. (13), ν is the reduction factor (ν depends on the importance class of the buildings). The corresponding reduction factor ν equals 0.5. α is a factor that takes the nonstructural elements into consideration and their adjustment

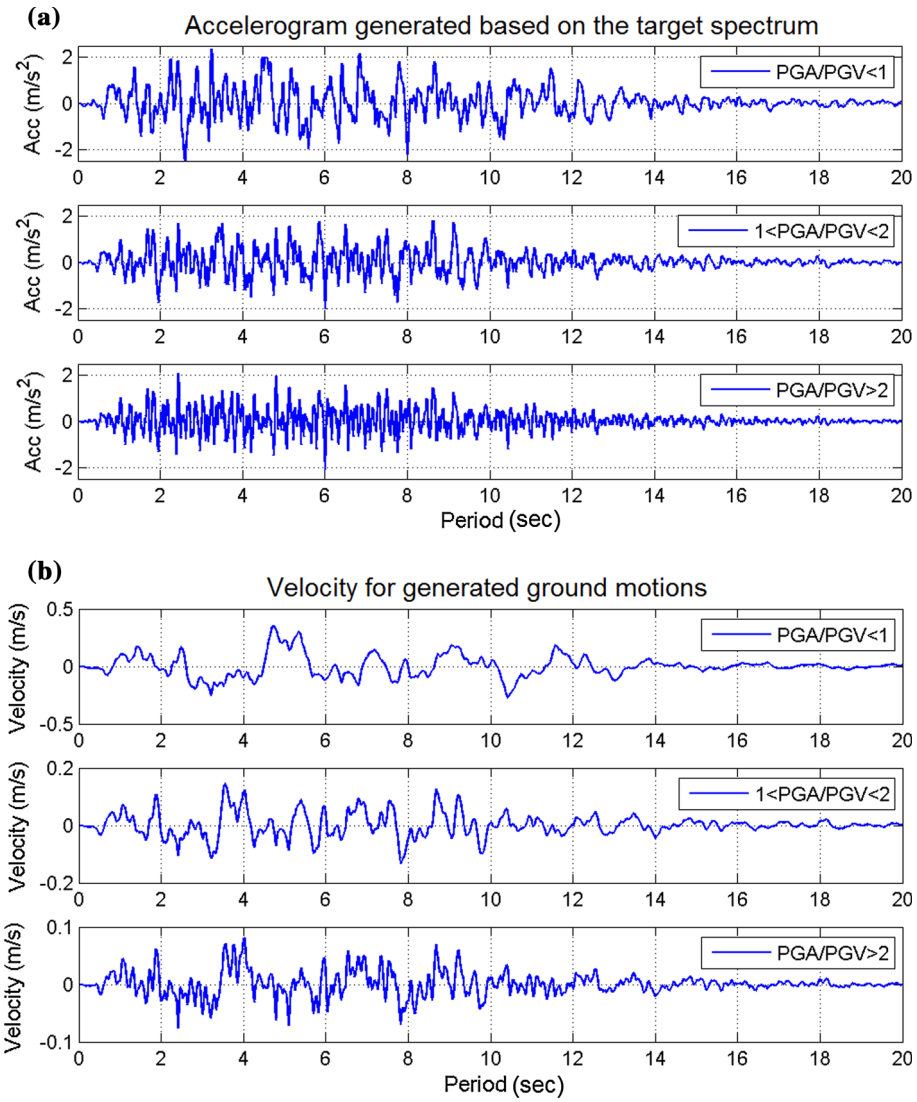

Fig. 17 **a** Accelerogram generated based on the target spectrum for each group (see also Fig. 5) and **b** velocity–time history based on the generated accelerogram

Table 7 Peak ground responses for artificial generated ground motions based on median spectrum of the real ground motions

EQ case	PGA (m/s^2)	PGV (m/s)	PGD (m)	PGA/PGV	Ratio
1	0.28	0.351	0.152	0.763	PGA/PGV < 1
2	0.203	0.145	0.039	1.4	1 < PGA/PGV < 2
3	0.212	0.081	0.023	2.61	PGA/PGV > 2

into the subject buildings, which equals 0.5, 0.75 and 1% [26].

Figure 23 illustrates the drifts for both base-isolated and fixed-base states. As it is clear, by increasing the number of stories, the effects of the base isolation system are reduced, but regarding the damage limitation requirement, it can be realized that by the existence of the base isolation system, especially for high-rise buildings, the structure is highly affected, which keeps the damage limitation requirement below 1%. The most severe drift limit ($\frac{\alpha}{\upsilon} = 0.01$, there are nonstructural elements in the building that are forced to be stable under structural deformation) is not exceeded in any story for base-isolated buildings, which causes the structure to remain within the elastic range. Additionally, story drifts are significantly decreased for base-isolated buildings, even for very high buildings.

5 Conclusions

Seismic isolation systems have been used as alternative lateral force resisting methods that have the potential to protect nonstructural and structural components. While many control systems have been proposed not only for response

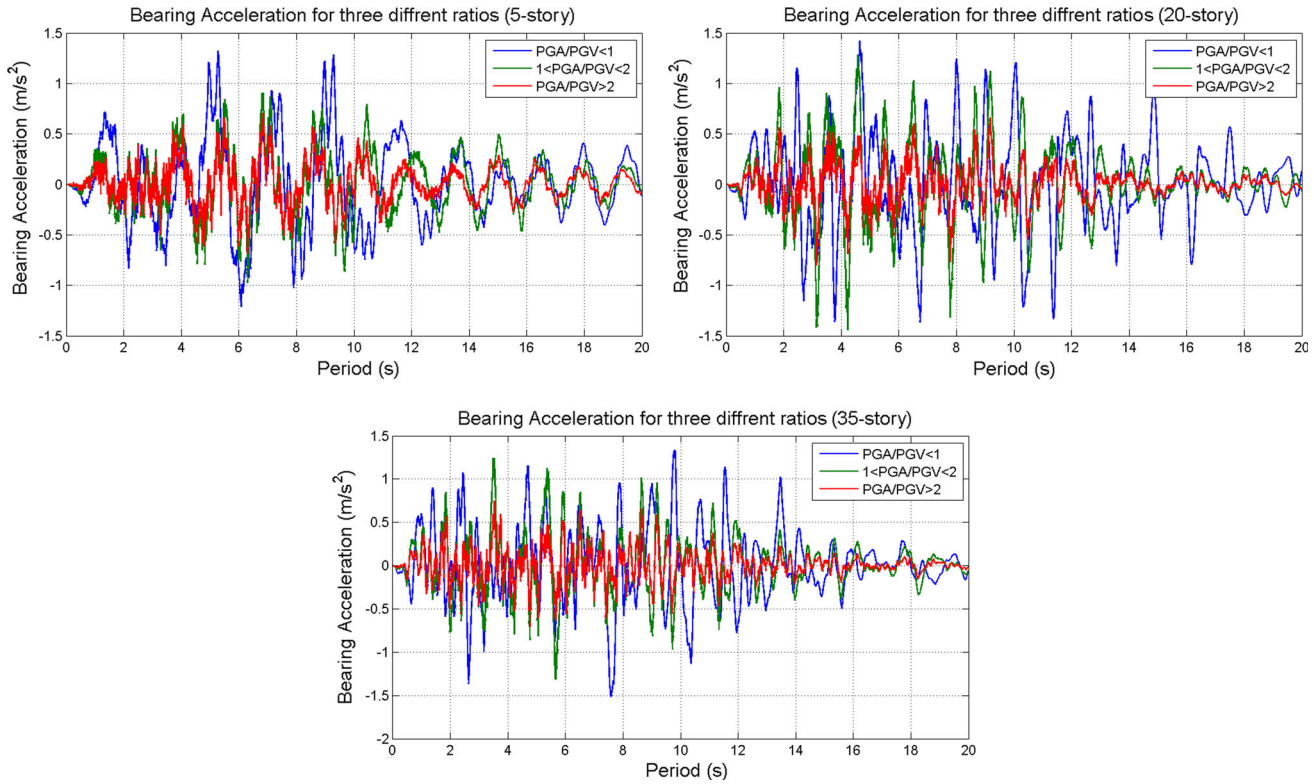

Fig. 18 Absolute acceleration of the bearing

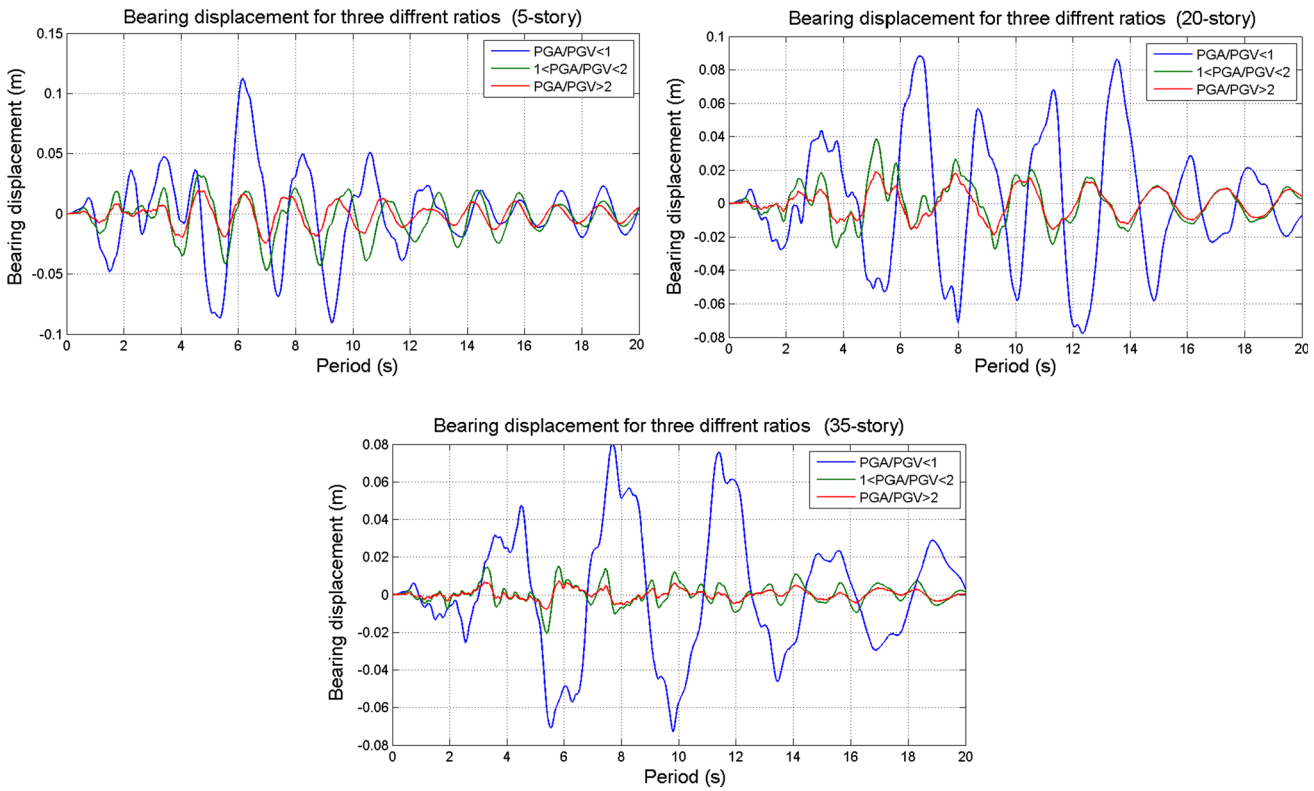

Fig. 19 Relative displacement of the bearing

Table 8 Bearing displacement and acceleration results for generated ground motions based on median spectrum of the real ground motions

EQ group (case)	5-Story		20-Story		35-Story	
	Dis.	Abs. Acc.	Dis.	Abs. Acc.	Dis.	Abs. Acc.
1	0.112	1.319	0.0881	1.427	0.080	1.512
2	0.047	0.976	0.0385	1.439	0.020	1.315
3	0.024	0.706	0.0189	0.797	0.0078	0.747

Abs. Acc absolute acceleration (m/s^2), *Dis* displacement (m)

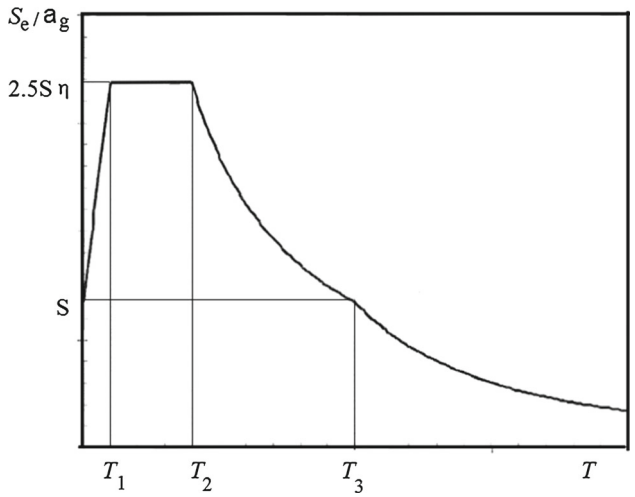

Fig. 20 Form of the elastic response spectrum [26]

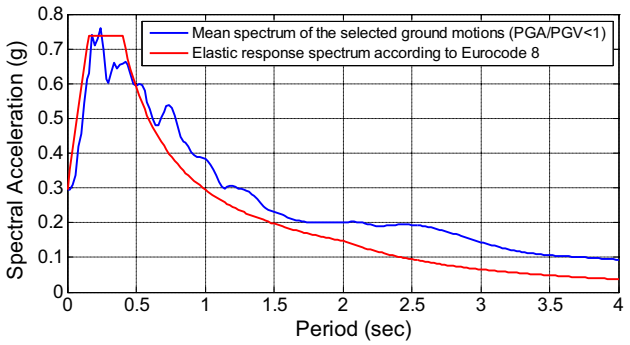

Fig. 21 Mean response spectrum of the selected earthquakes (PGA/PGV < 1) and elastic response spectrum according to Eurocode 8 for 5% damping

reduction in base-isolated buildings under different strong ground motions but also to maintain a safety function of base isolation systems to reduce the effects of large accelerations induced by the ground motions, these systems still seem to be quite complicated to use. Consequently, in this research, the behaviors of base-isolated buildings and base isolation systems under various ground motions with different components were investigated. The following are the main outcomes of this assessment:

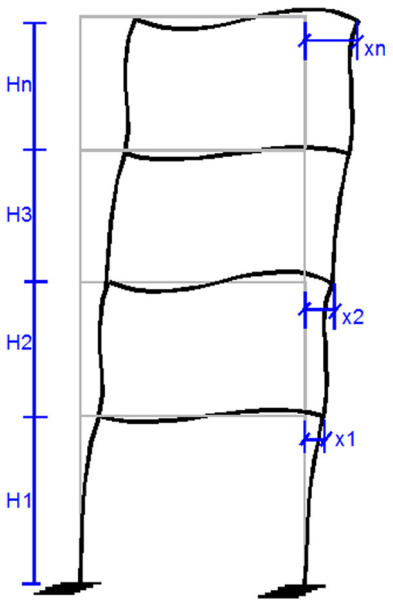

Fig. 22 Story drift

(1) There is a significant decrease in the top floor displacement for the three cases of PGA/PGV compared to fixed-base buildings (i.e., 5-, 10-, 15-, 20- and 25-story buildings), but the results are inverse for 30- and 35-story buildings, and the displacements in the base-isolated buildings are higher than those in the fixed-base buildings. Moreover, acceleration of the top floor of the base-isolated building is also decreased for the three cases mentioned above when compared to the acceleration of the top floor of the fixed-base building, but it remains unchanged for the 30- and 35-story buildings. In other words, in low-rise structures, there is a considerable decrease in the acceleration at the top floor of the base-isolated buildings for all three different cases. In addition, it can be concluded that the influence of the isolator system is decreased as the number of stories increase.

(2) By increasing the number of stories, the ratio of the base isolator displacement to PGD and the ratio of the top floor displacement to the PGD behave inversely. In other words, the ratio of the base isolation displacement to PGD is higher for low-rise buildings, but when com-

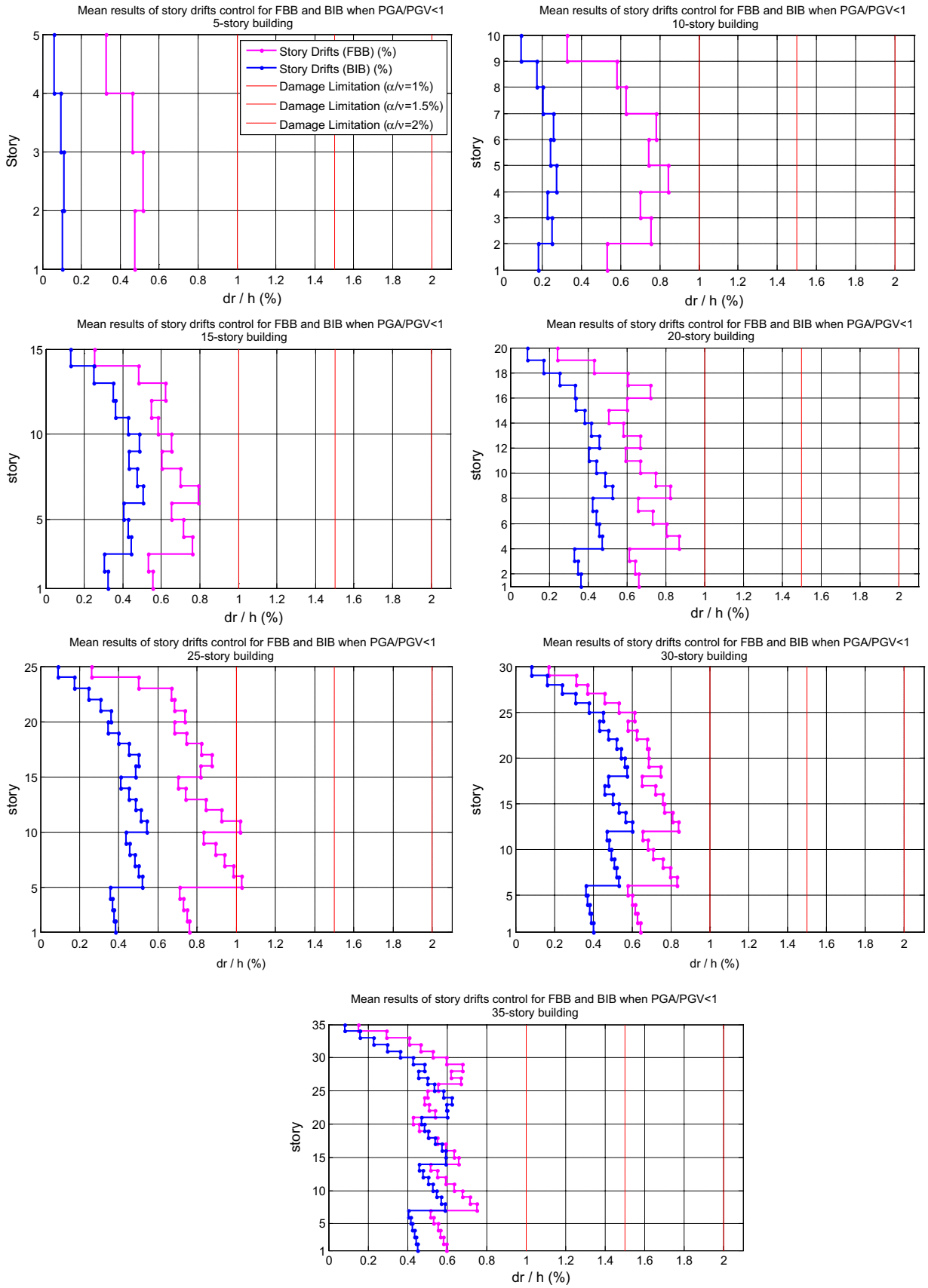

Fig. 23 Story drift control for seven different isolated buildings

pared with the ratio of the top floor displacement to PGD, this ratio for low-rise buildings becomes smaller.

(3) For different high-rise base-isolated buildings, the acceleration of the isolation system is reduced approximately 55% with reference to the PGA for three cases of PGA/PGV.

(4) For the three cases of PGA/PGV, as the ratio increases, the amount of energy dissipation is decreased by the base isolation system.

(5) The acceleration of the isolation system compared to the PGA is decreased for the three cases of PGA/PGV (as the ratio increases). In contrast, the displacement of the isolation system with reference to the PGD increased for the mentioned cases in order.

(6) According to the accelerogram generated based on the target spectrum for each case of the ground motions (see Fig. 17) and the bearing displacements observed for these kinds of earthquakes, it can be concluded that as the ratio of PGA/PGV decreases, the bearing displacement is sharply increased for 35-story base-isolated building in the case when PGA/PGV < 1 (see Fig. 19). Therefore, the base-isolated high-rise buildings (i.e., 20-, 25-, 30- and 35-story) can be vulnerable to the ground motions when PGA/PGV ratio is smaller than 1.

(7) As was observed, by increasing the number of the stories, the effects of the base isolation system are reduced; however, considering the damage limitation criteria, it can be observed that the effects of the base isolation system, especially for high-rise buildings, are highly observable and keep the damage limitation requirement below 1%. Furthermore, story drifts are significantly decreased for base-isolated buildings even for truly high-rise ones (i.e., 25-, 30-, 35-story).

Note that this study mainly investigates the LCRB base isolator, and different isolation systems could have different results. Thus, the three levels for the damage limitation requirement herein might not be appropriate for other types of isolation systems. Moreover, as the base-isolated buildings and base isolation systems are period dependent, investigating their seismic behavior under velocity pulse period ground motions can be a part of future study.

References

1. Castaldo, P.; Palazzo, B.; Della, V.P.: Seismic reliability of base-isolated structures with friction pendulum bearings. Eng. Struct. **95**, 80–93 (2015). https://doi.org/10.1016/j.engstruct.2015.03.053
2. Tavakoli, H.R.; Naghavi, F.; Goltabar, A.R.: Dynamic responses of the base-fixed and isolated building frames under far- and near-fault earthquakes. Arab. J. Sci. Eng. **39**(4), 2573–2585 (2014). https://doi.org/10.1007/s13369-013-0891-8
3. Choun, Y.S.; Park, J.; Choi, I.K.: Effects of mechanical property variability in lead rubber bearings on the response of seismic isolation system for different ground motions. Nucl. Eng. Technol. **46**(5), 605–618 (2014). https://doi.org/10.5516/NET.09.2014.718
4. Alhan, C.; Sahin, F.: Protecting vibration-sensitive contents: an investigation of floor accelerations in seismically isolated buildings. Bull. Earthq. Eng. **9**(4), 1203–1226 (2011). https://doi.org/10.1007/s10518-010-9236-0
5. Sayani, P.J.; Ryan, K.L.: Comparative evaluation of base-isolated and fixed-base buildings using a comprehensive response index. J. Struct. Eng. **35**, 698–707 (2009). https://doi.org/10.1061/(ASCE)0733-9445(2009)135:6(698)
6. Mazza, F.; Vulcano, A.: Nonlinear response of RC framed buildings with isolation and supplemental damping at the base subjected to near-fault earthquakes. J. Earthq. Eng. **13**, 690–715 (2009). https://doi.org/10.1080/13632460802632302
7. Harvey, P.S.; Gavin, H.P.: Assessment of a rolling isolation system using reduced order structural models. Eng. Struct. **99**, 708–725 (2015). https://doi.org/10.1016/j.engstruct.2015.05.022
8. Alhan, C.; Davas, S.Ö.: Performance limits of seismically isolated buildings under near-field Earthquakes. Eng. Struct. **116**, 83–94 (2016). https://doi.org/10.1016/j.engstruct.2016.02.043
9. Matsagar, V.A.; Jangid, R.S.: Influence of isolator characteristics on the response of base-isolated structures. Eng. Struct. **26**, 1735–1749 (2004). https://doi.org/10.1016/j.engstruct.2004.06.011
10. Samali, B.; Wu, Y.M.; Li, J.: Shake table tests on a mass eccentric model with base isolation. Earthq. Eng. Struct. Dyn. **32**, 1353–1372 (2003). https://doi.org/10.1002/eqe.277
11. Jangid, R.S.: Optimum lead–rubber isolation bearings for near-fault motions. Eng. Struct. **29**, 2503–2513 (2007). https://doi.org/10.1016/j.engstruct.2006.12.010
12. Mavronicola, E.; Polycarpou, P.; Papaloizou, L.; Komodromos, P.: Computer aided investigation of special issues of the response of seismically isolated buildings. Int. J. Comput. Methods Exp. Meas. **3**(1), 21–32 (2015). https://doi.org/10.2495/CMEM-V3-N1-21-32
13. Chimamphant, S.; Kasai, K.: Comparative response and performance of base-isolated and fixed-base structures. Earthq. Eng. Struct. Dyn. **45**, 5–27 (2016). https://doi.org/10.1002/eqe.2612
14. Takewaki, I.: Robustness of base-isolated high-rise buildings under code-specified ground motions. Struct. Des. Tall Spec. Build. **17**, 257–271 (2008). https://doi.org/10.1002/tal.350
15. Naeim, F.; Kelly, J.M.: Design of seismic isolated structures: from theory to practice, mechanical characteristics and modeling of isolators, pp. 93–121. Wiley, New York (1999)
16. Ikhouane, F.; Rodellar, J.: Systems with hysteresis analysis identification and control using the Bouc–Wen model. Wiley-Interscience, New York (2007)
17. Xu, C.; Chase, J.G.; Rodgers, G.W.: Physical parameter identification of nonlinear base-isolated buildings using seismic response data. Comput. Struct. **145**, 47–57 (2014). https://doi.org/10.1016/j.compstruc.2014.08.006
18. Elghazouli, A.Y.: Seismic Design of Buildings to Eurocode 8, 2nd edn. CRC Press, Boca Raton (2016)
19. Dormand, J.R.; Prince, P.J.: A family of embedded Runge–Kutta formulae. J. Comput. Appl. Math. **6**, 19–26 (1980)
20. Kulkarni, J.A.; Jangid, R.S.: Rigid body response of base-isolated structures. J. Struct. Control **9**, 171–188 (2002). https://doi.org/10.1002/stc.11
21. Kelly, J.M.: Earthquake-resistant design with rubber, 2nd edn. Springer, New York (1997). https://doi.org/10.1007/978-1-4471-0971-6
22. Alhamaydeh, M.H.; Barakat, S.A.; Abed, F.H.: Multiple regression modeling of natural rubber seismic-isolation systems with supplemental viscous damping for near-field ground motion. J. Civil Eng. Manag. **5**, 665–682 (2013). https://doi.org/10.3846/13923730.2013.799089

23. Eurocode 1, Actions on structures—part 1-1: general actions—densities, self-weight, imposed loads for buildings, EN 1991-1-1
24. Eurocode, Basis of structural design, EN1990
25. Saragoni, G.R.; Hart, G.C.: Simulation of artificial earthquakes. Earthq. Eng. Struct. Dyn. **2**, 219–267 (1973). https://doi.org/10.1002/eqe.4290020305
26. Eurocode 8, Design of structures for earthquake resistance-part 1: general rules, seismic actions and rules for buildings, EN1998-1